

1-1-2007

Development of in-cylinder injection for a hydrogen-fueled internal combustion engine

Ronald L Fifield

University of Nevada, Las Vegas

Follow this and additional works at: <https://digitalscholarship.unlv.edu/rtds>

Repository Citation

Fifield, Ronald L, "Development of in-cylinder injection for a hydrogen-fueled internal combustion engine" (2007). *UNLV Retrospective Theses & Dissertations*. 2232.

<http://dx.doi.org/10.25669/mbz5-7mrh>

This Thesis is protected by copyright and/or related rights. It has been brought to you by Digital Scholarship@UNLV with permission from the rights-holder(s). You are free to use this Thesis in any way that is permitted by the copyright and related rights legislation that applies to your use. For other uses you need to obtain permission from the rights-holder(s) directly, unless additional rights are indicated by a Creative Commons license in the record and/or on the work itself.

This Thesis has been accepted for inclusion in UNLV Retrospective Theses & Dissertations by an authorized administrator of Digital Scholarship@UNLV. For more information, please contact digitalscholarship@unlv.edu.

DEVELOPMENT OF IN-CYLINDER INJECTION FOR
A HYDROGEN-FUELED INTERNAL
COMBUSTION ENGINE

by

Ronald L. Fifield

Bachelor of Science, 2005
University of Nevada, Las Vegas

A thesis submitted in partial fulfillment
of the requirements for the

Master of Science Degree in Mechanical Engineering
Howard R. Hughes College of Engineering
Department of Mechanical Engineering

Graduate College
University of Nevada, Las Vegas
December 2007

UMI Number: 1452243

INFORMATION TO USERS

The quality of this reproduction is dependent upon the quality of the copy submitted. Broken or indistinct print, colored or poor quality illustrations and photographs, print bleed-through, substandard margins, and improper alignment can adversely affect reproduction.

In the unlikely event that the author did not send a complete manuscript and there are missing pages, these will be noted. Also, if unauthorized copyright material had to be removed, a note will indicate the deletion.

UMI[®]

UMI Microform 1452243

Copyright 2008 by ProQuest LLC.

All rights reserved. This microform edition is protected against unauthorized copying under Title 17, United States Code.

ProQuest LLC
789 E. Eisenhower Parkway
PO Box 1346
Ann Arbor, MI 48106-1346



Thesis Approval
The Graduate College
University of Nevada, Las Vegas

November 9, 2007

The Thesis prepared by

Ronald L. Fifield

Entitled

Development of In-Cylinder Injection for a Hydrogen-Fueled Internal
Combustion Engine

is approved in partial fulfillment of the requirements for the degree of

Master of Science in Mechanical Engineering

Examination Committee Chair

Dean of the Graduate College

Examination Committee Member

Examination Committee Member

Graduate College Faculty Representative

ABSTRACT

Development of In-Cylinder Injection for a Hydrogen-Fueled Internal Combustion Engine

by

Ronald Fifield

Dr. Robert Boehm, Examination Committee Chair
Distinguished Professor of Mechanical Engineering
University of Nevada, Las Vegas

Traditional means for converting an engine to operate on hydrogen fuel incorporates port injection. The typical method for controlling emissions on a port injection engine is to operate the engine lean (typical AFR of 70:1) and/ or incorporate an EGR system. The result of utilizing these methods is an appreciable reduction in power output. In-cylinder injection of an internal combustion engine provides a reliable method for delivering hydrogen fuel whereby fuel efficiency, power output and emissions levels are improved. Injection of hydrogen directly into the combustion chamber allows control of various factors such as burn rate and combustion timing which influence the production of emissions in the form of NO_x. Testing of the converted engines has also shown an increase in power due to an increase in volumetric efficiency and a reduction of emissions at near stoichiometric operation. Details for converting an engine to an in-

cylinder hydrogen injection, computer systems control, emissions testing and performance evaluation are given.

TABLE OF CONTENTS

LIST OF FIGURES	vii
LIST OF TABLES	ix
CHAPTER 1 INTRODUCTION	1
Justification of Project	1
CHAPTER 2 LITERATURE REVIEW	5
Hydrogen Embrittlement	5
Theory and Simulation.....	6
Effects on Alloys.....	10
Preventing Hydrogen Embrittlement	11
Hydrogen Motor Conversions	12
Conversion	12
Emissions Characteristics of Hydrogen Engines	15
Injection System Design	17
CHAPTER 3 DESIGN CRITERIA	21
Engine Modification	21
Engine Simulations	22
Computer Modification.....	26
Spark Modifications.....	27
Fuel Modifications.....	28
Injector Design.....	29
CHAPTER 4 COMPONENT DESIGN.....	30
Polaris Engine	30
Check Valve.....	30
Timing Components.....	38
Ford Engine.....	39
High Pressure Injector.....	39
Design of Internal Valve.....	44
CHAPTER 5 VEHICLE CONVERSION	48
Polaris Conversion.....	48
Electrical System	50
Fuel System.....	52
Ford Conversion	54
CHAPTER 6 TESTING AND ANALYSIS	56

Performance	56
Emissions	63
Baseline Emissions Testing	63
Emissions for Direct Injection of Hydrogen.....	65
CHAPTER 7 DISCUSSION AND CONCLUSIONS	68
APPENDIX I TABLES OF ENGINE PARAMETERS AND C_v TEST RESULTS.....	72
APPENDIX II MATHCAD SIMULATION OF EMISSIONS FOR 425CC ENGINE..	74
APPENDIX III TEST DATA FOR EXTERNAL COIL OPERATION AT 12, 18, AND 24 VDC	77
APPENDIX IV TEST EQUIPMENT.....	79
REFERENCES	80
VITA.....	84

LIST OF FIGURES

Figure 2-1	Schematic of possible reaction steps involved in the embrittlement of a structural alloy by external molecular hydrogen environment [2] [7].	7
Figure 2-2	The effect of hydrogen on cavity nucleation, cavity linkage and fracture of the specimen [3].	8
Figure 2-3	Variation of preheat temperature with volume % of hydrogen in the shielding gas [7] [8].	9
Figure 2-4	Minimum ignition energies for various fuels [17] [22].	13
Figure 2-5	Thermal efficiencies and where backfiring occurs for an external mixture and direct-cylinder injection with varying percentages from each. [18].	15
Figure 2-6	Effects of injection timing θ_j on volumetric efficiency for different equivalence ratios. [19].	16
Figure 2-7a	Electrical equivalent of solenoid.	20
Figure 2-7b	Mechanical equivalent of solenoid	20
Figure 2-8	Section drawing of test solenoid	20
Figure 3-1	Ford modular head showing sparkplug bore extending through valve cover to center of combustion chamber.	22
Figure 3-2	Simulation of emissions for a 425cc single cylinder engine.	24
Figure 3-3	Simulation of adiabatic flame temperature for a 425cc single cylinder engine.	24
Figure 3-4	Torque profile of a single cylinder motor	25
Figure 3-5	Engine timed events superimposed on camshaft cycle	25
Figure 4-1	Stress in the hoop direction for a cylinder	35
Figure 4-2	Measurement for check valve impact fatigue diagram	36
Figure 4-3	Section view of Polaris check valve	37
Figure 4-4	Polaris engine with fueling modifications	37
Figure 4-5	Camshaft timing components for Polaris motor	38
Figure 4-6	Crankshaft timing components for Polaris motor	39
Figure 4-7	Section view of sparkplug injector with external solenoid valve	40
Figure 4-8	Section view of sparkplug injector test module	41
Figure 4-9	Polaris cylinder head cutaway	42
Figure 4-10	Critical point on gas coupler assembly	43
Figure 4-11	Critical points on housing	44
Figure 4-12a	Section view of test fixture for internal pressure valve.	46
Figure 4-12b	Test fixture for internal high pressure valve	46
Figure 4-13a	Section view of external coil, high pressure valve	47
Figure 4-13b	Test fixture for external coil, high pressure valve	47
Figure 5-1	Polaris vehicle final conversion	49
Figure 5-2	Engine compartment of Polaris engine	50

Figure 5-3	Wiring scheme of Polaris relay box.....	51
Figure 5-4	Relay box position under hood of Polaris vehicle	52
Figure 5-5	Polaris fuel cutoff valve, pressure regulator, dump valve and PVD.....	53
Figure 5-6	Fill connector and tank pressure gauge on Polaris vehicle	54
Figure 5-7	Ford vehicle to be converted.....	55
Figure 6-1	Fuel and volumetric efficiencies for hydrogen at WOT	60
Figure 6-2	Volumetric and fuel efficiencies for gasoline at WOT, $\Phi = 1$	61
Figure 6-3	Volumetric and fuel efficiencies for CNG at WOT, $\Phi = 1$	61
Figure 6-4	Power output of hydrogen, CNG and gasoline	62
Figure 6-5	Power output for direct injection of hydrogen.....	62
Figure 6-6	Emissions for gasoline at WOT, RPM = 3000	63
Figure 6-7	Emissions for gasoline at WOT, RPM = 4000	64
Figure 6-8	Emissions for CNG at WOT, RPM = 3000	64
Figure 6-9	Emissions for CNG at WOT, RPM = 4000	65
Figure 6-10	Emissions for direct injection of hydrogen at MAP = 16 to 18 inHg.....	66
Figure 6-11	Emissions for direct injection of hydrogen at MAP = 20 to 24 inHg.....	66
Figure 6-12	Emissions for direct injection of hydrogen at WOT	67

LIST OF TABLES

Table 1-1	Nomenclature	3
Table 3-1	Typical timing events for hydrogen engine	26
Table 3-2	Optimized ignition angle for Polaris motor	28
Table 4-1	Combustion chamber temperature due to polytropic compression.....	32
Table 4-3	Safety factor of critical points of Polaris check valve	35
Table 4-4	Safety factor of critical point for sparkplug injector.....	42
Table 6-1	BSFC of various fuels at WOT	58
Table 6-2	LHV of fuels	59
Table 6-3	Engine efficiency of various fuels at WOT using BSFC and LHV	59
Table AI-1	Specifications for 425cc Polaris engine	72
Table AI-2	Polaris check valve flow data for air.....	72
Table AI-3	Check valve seat test data	73
Table AIII-1	External coil at 12 VDC.....	77
Table AIII-2	External coil at 18 VDC.....	77
Table AIII-3	External coil at 24 VDC.....	78
Table AIV-1	Testing instruments by manufacturer.....	79

CHAPTER 1

INTRODUCTION

The Hydrogen Refilling Station Project, located on the grounds of the Las Vegas Valley Water District (LVVWD), brought about novel design considerations for both emissions control as well as advancements in control over the fuel delivery system. Traditional means for converting a gasoline engine to operate on gaseous hydrogen fuel is to inject the fuel into the intake manifold, otherwise known as port injection. While port injection is an effective means for delivering fuel, various parameters pertinent for utilizing the full potential of hydrogen must be ignored. For instance, to eliminate pre-ignition or backfire through the intake system the air fuel ratio (AFR) is leaned out. It is understood that to effectively control hydrogen specific parameters such as burn rate, power density, emissions, etc. an accurate control of timing events such as the fuel delivery and spark is needed. Because of the inherent design of a direct injection system, control over fuel delivery is easily accomplished. While direct injection (DI) has been around for a number of years, the concept utilized for H₂ICE's are still in the infancy.

Justification of Project

The converted vehicles developed for this project are to be used at the LVVWD by maintenance personal including grounds personal at the Springs Preserve. Proof of concept as well as reliability testing will ensure the conversion is suitable for use in this environment. The development of a DI injector provides a suitable platform whereby

advancements in the computer control were refined as well as innovative designs including a sparkplug/ injector were developed; development and testing of one such sparkplug/ injector is described herein.

Table 1-1 Nomenclature

Symbol	Definition
ABDC	After Bottom Dead Center
AFR	Air Fuel Ratio
ATDC	After Top Dead Center
BDC	Bottom Dead Center
BMEP	Brake Mean Effective Pressure
BSFC	Brake Specific Fuel Consumption
BTDC	Before Top Dead Center
CNG	Compressed Natural Gas. Methane (CH ₄) for simplicity
CR	Compression Ratio
ECM	Engine Control Module
EGT	Exhaust Gas Temperature
HAZ	Heat Affected Zone
ICE	Internal Combustion Engine
k	Ratio of Specific Heats
LED	Light Emitting Diodes
LHV	Lower Heating Value
MAP	Manifold Absolute Pressure
NO _x	Nitrous Oxide- Can take the form of NO or NO ₂
ppm	Parts Per Million
PRD	Pressure Relief Device
PRV	Pressure Relief Valve
Phi (Φ)	Equivalence Ratio
	Φ < 1 → Lean
	Φ > 1 → Rich
	Φ = 1 → Stoichiometric

RPM Revolutions Per Minute (Engine speed)

T Final Temperature

TDC Top Dead Center

To Initial Temperature

TPI Throttle-body Port Injection

VDC Volts- Direct Current

WOT Wide Open Throttle

CHAPTER 2

LITERATURE REVIEW

Hydrogen Embrittlement

With the increasing demand for alternative fuel(s), hydrogen as a replacement to gasoline has recently come to the forefront of studies. This particular study involves the conversion of gasoline powered ICE with emphasis on design of the injection system and controls to operate on hydrogen gas. To examine the effects such a conversion would also require a complete understanding of the impact the new medium would present on the system. In particular, it would be worthwhile to know how existing engine components as well as the newly designed components would behave in the presence of hydrogen gas. As will be shown, various environments, such as high moisture content, also contribute to accelerated hydrogen embrittlement. The combustion of hydrogen gas, H_2 , and air (22% O_2) yields water, H_2O , and energy in the form of heat.

While it can be shown that metals and alloys, regardless of composition, are susceptible to hydrogen embrittlement, various alloys behave differently and, to a great extent, predictably for a given environmental situation. Depending on the given scenario, it is possible to design a system that will limit either the damage created by failure in a material due to hydrogen embrittlement or delay the effects. For the conversion of the ICE, various external components could be classified as expendable in comparison to internal components such as the crankshaft or piston where failure would result in the

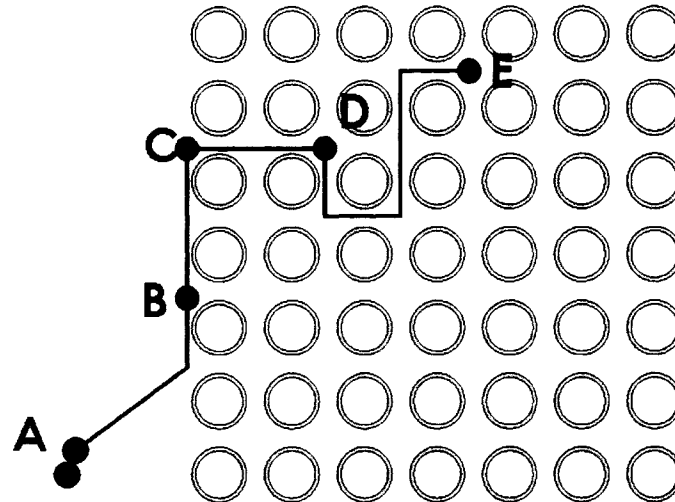
complete loss of the entire engine. For this reason, particular interest lies with how various alloys, both ferrous and non-ferrous materials, hold up to stresses in the presence of hydrogen gas. Component materials of interest in this particular study consist of 6061 T6, 2024 T6, 4043 steel, 316 and 303 SS.

Theory and Simulation

While various techniques and experiments have been used to describe the process of hydrogen embrittlement, metallurgical models have yet to qualitatively simulate the process. What is known is stated by Serebrinsky [1]; hydrogen embrittlement occurs by a three step process; 1) hydrogen is dissolved into the interstitial lattice, 2) the hydrogen travels to voids or vacancies whereby the hydrogen propagates the stress around the crack tip, and 3) propagation of stresses and the transportation of the hydrogen throughout the lattice leads to localized failure of metal. This process is represented in Figure 2-1.

In a study performed at Chugoku National Industrial Research Institute 0 a single crystal of iron, on a nanometer scale was examined. A 3-D model, on a microscopic scale of pure iron, was constructed to simulate the molecular dynamics hydrogen would have on a single crystal of iron. Computer simulation showed that plastic deformation occurred at 21,000 steps for samples without hydrogen; however the hydrogen charged specimen indicated fracture in as few as 7,000 steps. With this simulation, they were able to quantify inner-atomic action force in the presence of hydrogen. In a related study by Bettis Atomic Power Laboratory 0, a computer simulation to investigate intergranular stresses of Ni-based alloys. Sought was a model for predicting how the presence of hydrogen, through electrochemical reactions and solid-state diffusion affects the intergranular bonds. Also seen in the simulations is how the grain orientation greatly

influences the material's susceptibility to cracking. Because an alloy was used in these sets of simulations rather than a pure crystal, as shown previously, the question of how heat treatments, varying alloys composition and material preparations would be affected by hydrogen embrittlement.



Reaction steps: Diatomic hydrogen diffuse through ferrous material

A → B	Diffusion and dissociation
B → C	Migration
C → D	Solution
D → E	Lattice diffusion

Figure 2-1 Schematic of possible reaction steps involved in the embrittlement of a structural alloy by external molecular hydrogen environment [2] [7].

Kimura [5] from the National Institute for Materials Sciences, Japan, hypothesized that grain size played a critical role in localized failures of medium-carbon martensitic steels subjected to hydrogen. Through controlled temperature multi-pass bar rolling, a consistent 3 μm grain size is achieved for samples to be tested. Furthermore, these samples were subjected to various heat treatments resulting in varying diameters of undissolved carbides and grain sizes. Studies show that in the presence of carbides, residual stresses are present, however, when hydrogen is introduced methane is formed

from the bonding of the hydrogen to the carbide. This would present as blistering resulting in cracks. Samples were then exposed to hydrogen via electrically charging 3% NaCl + 0.3% NH₄SCN in a 0.1N NaOH aqueous solution. Results showed a direct correlation to diffusible hydrogen content and time to stress failure; failure time increases as the diffusible hydrogen content decreased. Likewise, when comparing samples of differing grain sizes, it was noted that fracture in conventional quenched and tempered samples failed at hydrogen contents as low as 0.11 ppm whereas in fine-grain samples, failure occurred at concentrations of 0.24 ppm. Confirmed with studies presented in IEEE journal [6], it has also been shown that the harder the material or the more organized the grain structure the greater tendency to resist hydrogen embrittlement.

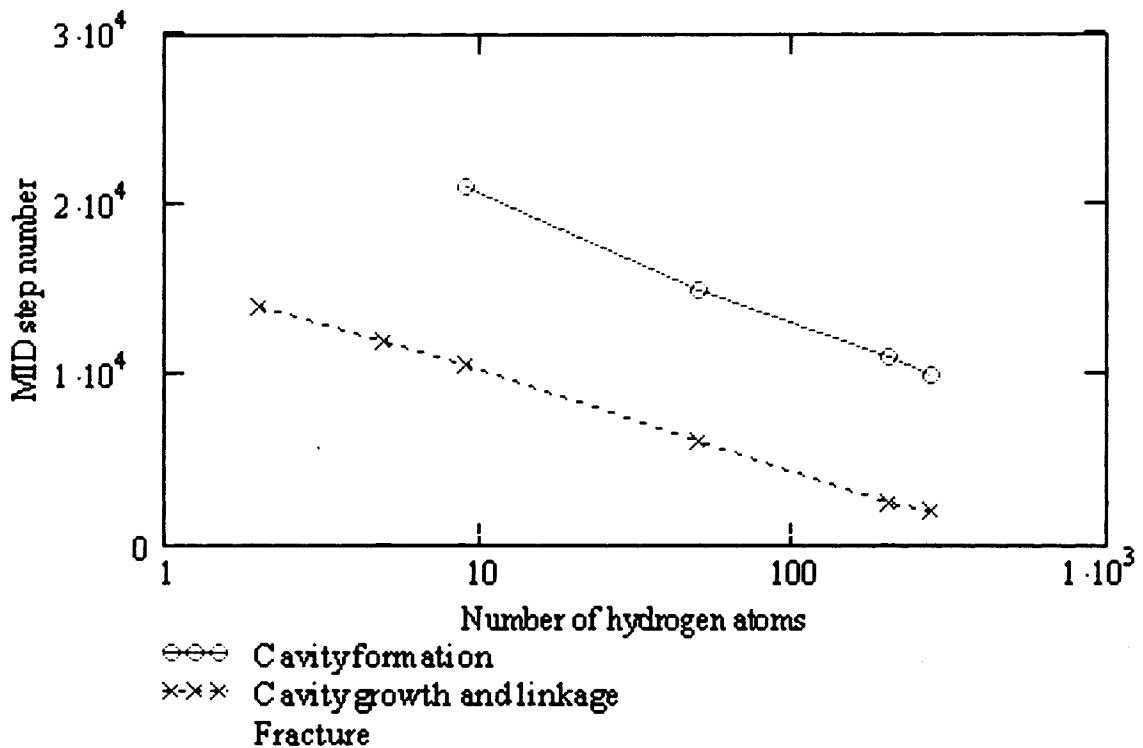


Figure 2-2 The effect of hydrogen on cavity nucleation, cavity linkage and fracture of the specimen 0.

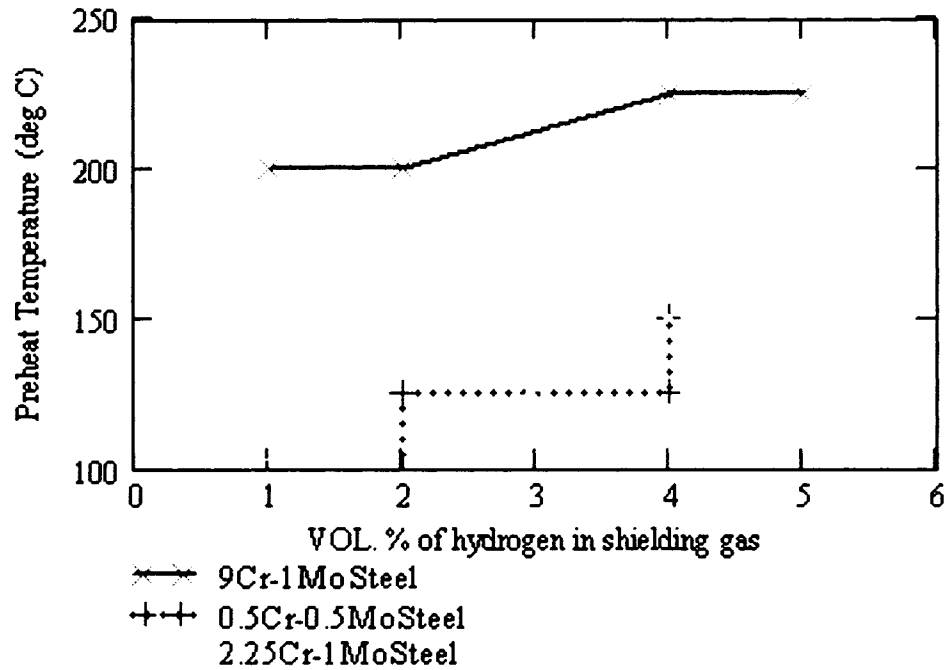


Figure 2-3 Variation of preheat temperature with volume % of hydrogen in the shielding gas [7] [8].

There are multiple methods for hydrogen to be absorbed into the metal. The most recognized method is due to the use of the metal in a corrosive environment, or any environment that would produce hydrogen gas through chemical reactions and/ or pure hydrogen gas. Other methods would include formation of the alloy, various heat treatments involving high moisture content as found in quenching, welding, and various others. The welding process involves liquefying the metal thus creating a molten pool. It is at this point that hydrogen is able to be absorbed. As the metal solidifies, solubility of hydrogen decreases due to the decrease in temperature thus causing the hydrogen presently in the weld to become supersaturated and diffuse to areas of lower concentration. The heat affected zone (HAZ), which is susceptible to regions of high hardness and low ductility, can undergo cracking in the presence of hydrogen within hours of completing the weld [7].

The various dependent variables of hydrogen embrittlement are “temperature, pressure, level and type(s) of stress, environment, physical and mechanical properties of bulk materials, type and concentration of impurities in the metal, thermo-mechanical history, hydrogen diffusion rate and surface conditions [7].” Pressure is attributed to the mode of failure due to diffusion of hydrogen into the metal and accumulation within the internal defects. The added pressure within the metal contributes as added stress and can promote crack growth. The surface conditions are believed to contribute by the lowering the free energy for crack growth due to the absorption of hydrogen adjacent to the crack tip.

Effects on Alloys

Hydrogen embrittlement is not confined to material with iron. In fact this phenomenon can be found in alloys not containing iron such as aluminum. Experiments conducted by Petroyiannis [10] and Lu [11] show aluminum to be extremely susceptible to hydrogen embrittlement. The work by Petroyiannis focuses on aircraft aluminum alloy 2024 T3 with failure due to hydrogen embrittlement in the absence of mechanical loading. Lu’s work [11] showed that hydrogen atoms are “trapped at vacancies in multiple numbers with rather high binding energies” and contribute to “superabundant vacancy formation in a number of metals, such as Pd, Ni, Cr, etc.” In these types of metals, it is speculated that up to six atoms of hydrogen can be trapped in a single vacancy. However, in aluminum, it is shown, from first principle calculations, that up to 12 hydrogen atoms can be trapped. Both Lu and Petroyiannis suggest that the consequence of the trapped hydrogen atom is low formation energy of the vacancy defect which in turn results in more formations of vacancies. Because hydrogen has the

tendency to collect in vacancies, there is a substantial increase in the solubility of hydrogen thus leading to hydrogen embrittlement which results in work hardening or tensile ductility decrease. Petroyiannis further concluded that ultimate and yield stress could be restored to the original values by mechanically removing the affected areas, however ductility required thermal treatment.

Preventing Hydrogen Embrittlement

Aside from heat treatments, various techniques have been employed to delay the effects of hydrogen embrittlement. The Institute of Material Engineering, National Chung Hsing University [12] applied electrolytic ZrO₂ coatings on stainless steel to investigate the retardation effects. Conclusions drawn from their experiments indicate that failure in the form of blistering can be significantly delayed through electrolyzing stainless steels with ZrO₂. Through mathematical models, and experiments to extrapolate various constants in the models, it was concluded that the delayed effect is due to relatively low concentrations of hydrogen in the metal; this too was concluded for materials like AL [10][11] as well as in mild steels 0.

Various industry techniques for manufacturing a quality product(s), presented in Dayal [7], give reasonable measures to limit the liability of hydrogen embrittlement. It is clearly understood that internal flaws such as blistering, shatter cracks, flakes, fish-eyes and porosity promote localized vacancies where hydrogen is allowed to accumulate and that in sufficient quantities, hydrogen produces these same flaws. Because the size of the atomic hydrogen limits the depth of penetration into the metals causing the defects, various finishing techniques have been developed to minimize the quantity of hydrogen in steels. Some of the various techniques utilized are vacuum melting, degassing,

avoidance of pickling or acid washing, and minimization of moisture content. Similarly, coatings in the form of oxides [12] on the finished material, welds and electrodes used in the welding or electro plating also help.

Hydrogen Motor Conversions

Hydrogen as a fuel provides an alternative to fossil fuels, however, with the exception of a small number of car manufactures few vehicles are produced with an H₂ICE. An alternative to purchasing a vehicle designed for use with hydrogen is to convert the engine. Research into the development of an engine fueled by hydrogen has been conducted on both diesel and gasoline engines with diesel preferred due to the relatively high compression ratios and a cylinder head design of two ports; one for the igniter/ glow plug and the other for the injector.

Conversion

Low ignition energies and a relatively high auto-ignition temperature for hydrogen coupled with a trend for a decrease in pre-ignition with an increase in the compression ratio [13] [14] [15] makes a diesel engine a good candidate for an engine to operate on hydrogen. In an experiment at Anna University [16] a diesel engine operating as a hybrid diesel/ hydrogen engine was chosen for these specific reasons.

In the experiments performed by Saravanan [16], hydrogen gas was passed to the combustion chamber via two methods; 1) carburetor and 2) TPI techniques. While a typical diesel engine utilized the compression cycle to raise the temperature sufficiently for combustion, a compression ratio of 16.5:1 and an injection pressure of 190 bars is not sufficient to cause ignition. That is to say the cooling effect of hydrogen expanding combined with and the increase in temperature due to the compression stroke is not

sufficient for the spontaneous combustion of hydrogen. Secondly, as this experiment used diesel as the ignition source and therefore hydrogen is mixed with the diesel; the specific heat ratios are much less than 1.41 and would therefore require temperatures above the auto-ignition temperature of hydrogen to ignite the mixture.

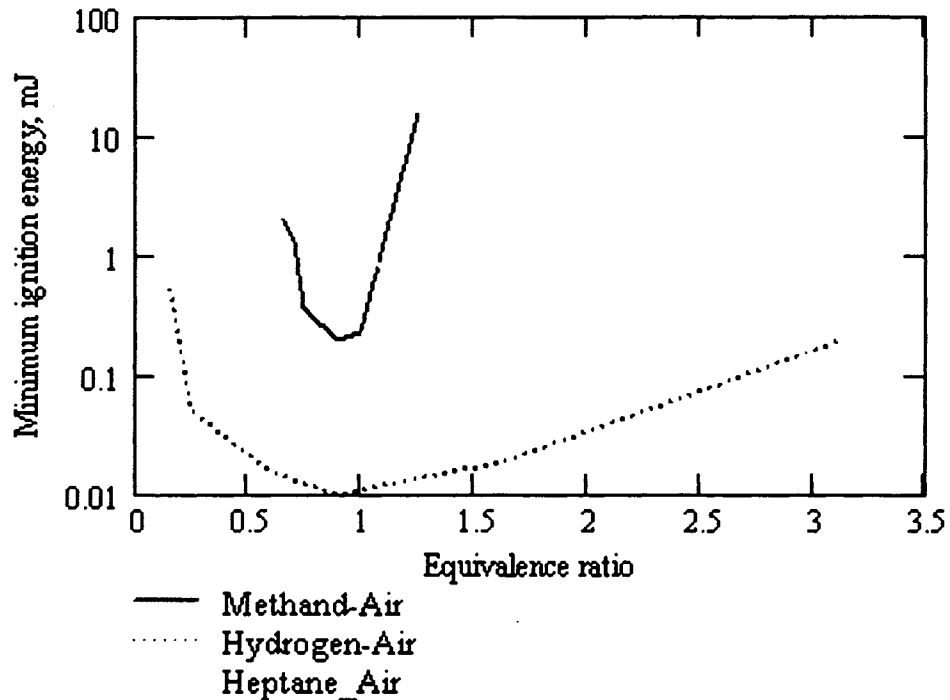


Figure 2-4 Minimum ignition energies for various fuels [17] [22].

The engine was initially started on diesel fuel then slowly limited as hydrogen gas was introduced. Performance and emissions were then compared to a baseline of diesel. Use of hydrogen in diesel motors shows improvements in areas of brake thermal efficiency, lower emissions such as the production of NO_x , smoke, hydrocarbons, carbon monoxides and dioxides.

To better understand backfiring, a case study was examined wherein a dual injection system was utilized to sort out the causes of backfiring. Lee [18] performed tests with a

dual injection system (port and direct injection) to determine the advantage of utilizing both technologies. Port injection is known for relatively high thermal efficiencies, however, this is limited to approximately 60% of full load. Direct injection is not necessary limited to the same loading issues as port injection as demonstrated in Figure 2-5. Thermal efficiency, oftentimes called fuel burn efficiency is a comparison of the maximum energy within a fuel (LHV) to the output of the engine. A lean running engine or homogeneous fuel/ air mixture tends to have a higher thermal efficiency. This is due to the lower flame propagation speed and larger thermal boundary which has a tendency, when compared to an engine operating at a lower thermal efficiency, to transfer more heat into power rather than wasted heat. The drawback with using direct injection is a lower thermal efficiency which is in part due to the short mixing period and higher flame front propagation speed. It was shown that early direct injection works better in achieving a more homogeneous mixture than late direct injection. This study also showed an increase of up to 60% higher torque by utilizing a dual injection system. By utilizing a dual injection system, this study was able to achieve maximum torque from a direct injection engine and high efficiencies from an external mixing engine. This study also showed a relationship between port injection pressure, injection timing, and prevalence to backfire. In short, optimum timing for port injection was determined to be at TDC. The relationship found for injection pressure and backfire occurrence was showed that as the injection pressure increases, the engine must be run leaner to minimize backfire. This study also showed a relationship between direct injection, thermal efficiency and torque. It was shown that injection prior to the closing the intake valve resulted in higher thermal efficiencies (due to greater mixing times) however, torque decreased due to a loss of

hydrogen into the intake and or the occurrence of backfiring. The thermal efficiencies tends to decrease as the injection occurred later (again due to the shortened mixing time) however, torque is essentially unchanged so as long as the intake valve is closed.

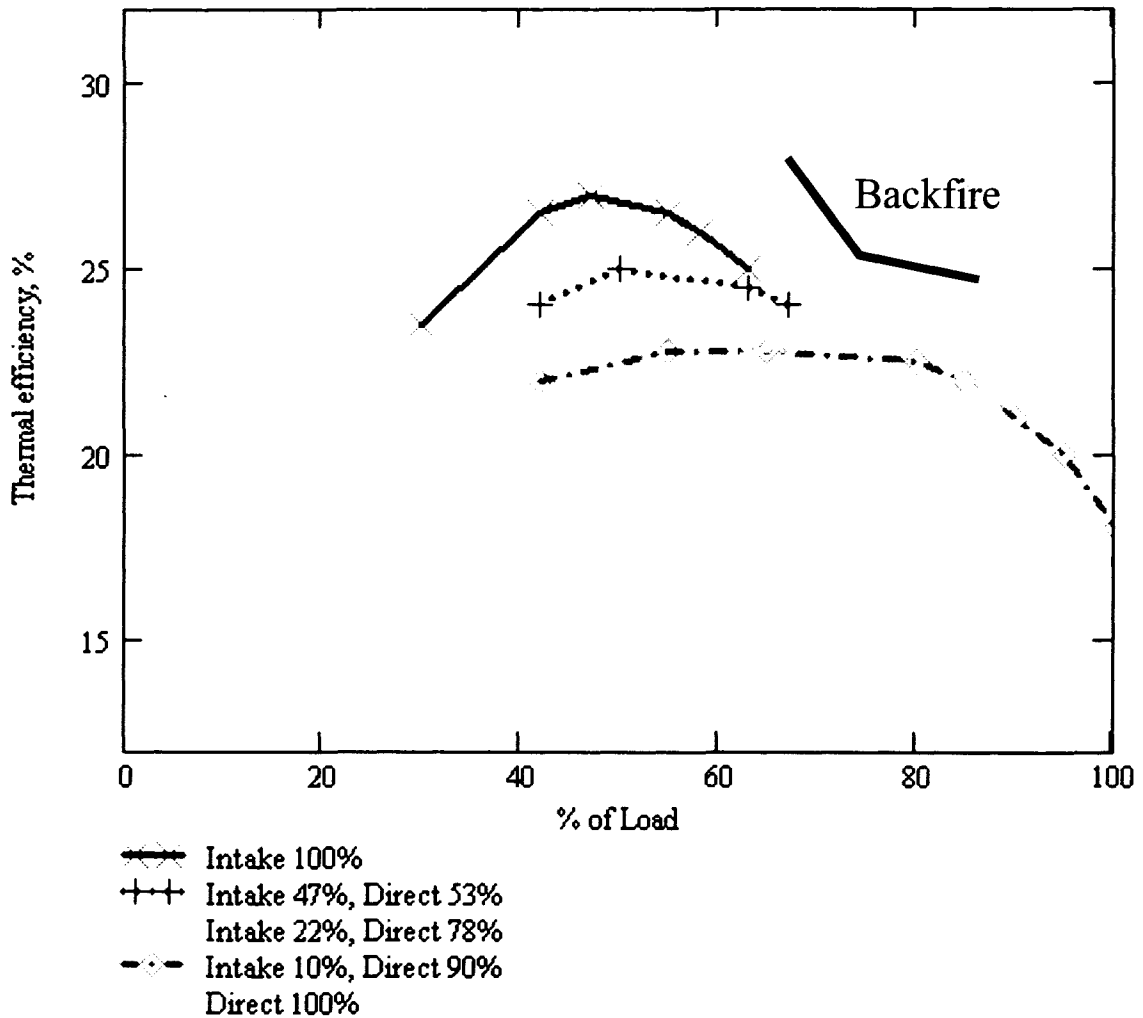


Figure 2-5 Thermal efficiencies and where backfiring occurs for an external mixture and direct-cylinder injection with varying percentages from each. [18]

Emissions Characteristics of Hydrogen Engines

Experiments performed by Mohammadi et al. [19] give emissions correlations between injection timing, thermal efficiencies, NO_x production, BMEP and cylinder

pressure. Also verified in Lee's [18] experiments is the tendency for an increase in volumetric efficiency as the injection timing is retarded up until the intake valve is completely closed. Demonstrated in Equations 2-1 and 2-2, by volume hydrogen can displace as much as 30% air if operating under stoichiometric conditions. Equation 2-1 is taken from the definition of AFR where the AFR is equal to the mass of air divided by the mass of the fuel. 'n' represents the number of moles in the mixture and 'mw' represents the corresponding molecular weight. Equation 2-2 is the mole fraction of the mixture within the combustion chamber. With these two equations, it is clearly deduced that if hydrogen is injected while the intake valve is open, regardless of port or direct injection, the tendency will be to displace air and consequently lower the volumetric efficiency. With less oxygen in the combustion process, less power can be made as compared to the same AFR but with more oxygen/ fuel.

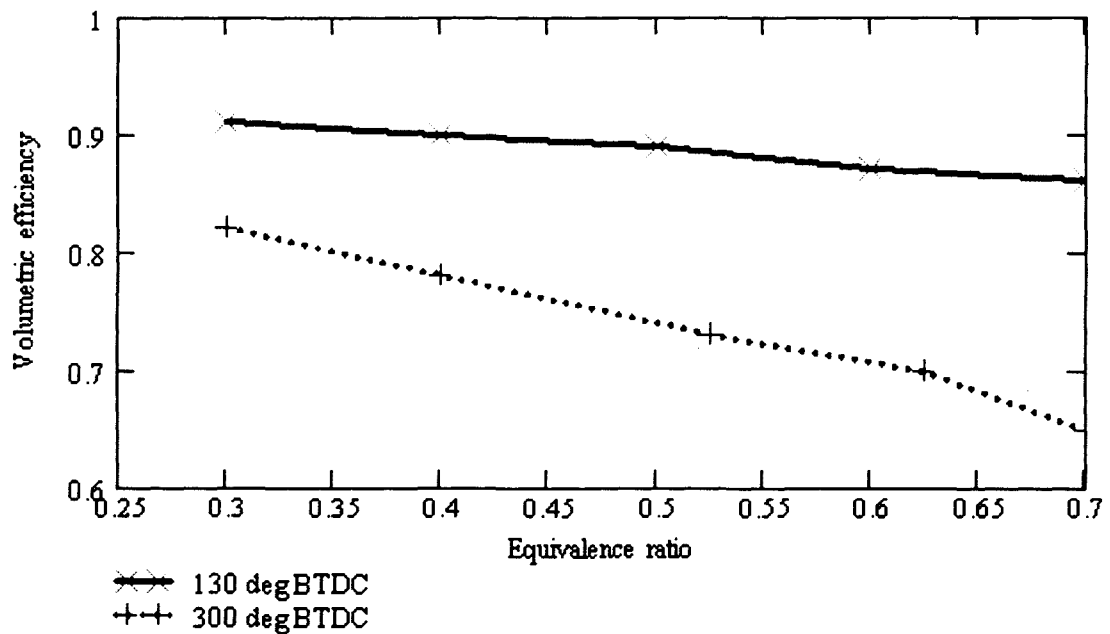


Figure 2-6 Effects of injection timing θ_j on volumetric efficiency for different equivalence ratios. [19]

$$n_{H2} = \frac{n_{Air} \cdot m_{wAir}}{m_{wH2} \cdot AFR} \quad (2-1)$$

$$y_{H2} = \frac{n_{H2}}{n_{Air} + n_{H2}} \quad (2-2)$$

Injection just after the intake valve has closed offers various benefits including higher thermal efficiency, elimination of backfires, limited knocks and improved volumetric efficiencies- precise timing of the injection event impacts emissions such as NO_x. Described by Mohammadi [19] are the effects of injection before and after the intake valve closes. The general trends noted for production of NO_x showed little production of NO_x for equivalence ratios below 0.5 and two orders of magnitude higher for equivalence ratios above 0.5. The thermal efficiencies, regardless of the injection point show maximum values for ignition points of approximately 10° BTDC. While maximum thermal efficiencies are achieved at 10° BTDC which corresponds to an equivalence ratio greater than 0.5 and production of emissions such as NO_x are higher at this point, consideration must be given when tuning the engine due to an increasing BMEP. Tradeoff concerning emissions production, thermal efficiency and maximum power output must be considered and ranked accordingly.

Injection System Design

The design of an injector is comprised of two main units; valve to meter the fuel and the body. The valve can have several forms such as a check valve coupled to a solenoid valve or even a solenoid valve with no check valve. The design of the solenoid valve should be sufficiently fast, accurate, and repeatable to deliver fuel in as short of time as 3 ms. Studies carried out by Kajima [20] examined the development of high speed

solenoids including the effect of switching speeds on armature mass, material types, and yoke and plunger designs.

The factor of most importance in this type of application is the switching time. Many factors influence switching time including material selection, yoke and plunger design, voltage and current levels, and the medium of operation. While theoretically it can be shown that a reduction in weight accounting for the skin effect, a condition where the magnetic flux localizes at the center of the material, will reduce switching time, experimentally it was shown to have negligible effects for reduction of mass up to 16%. Material selection is a critical factor when calculating switching times, magnetization and demagnetization time delays, and mitigation of eddy currents. In general it is understood that a material with a smaller electric conductivity produces a shorter switching time due to less eddy currents. The materials studied by Kajima [20] were Kawasaki Steel's RGH023, silicon steel, S10C, permalloy, and permendur. Through various experiments and mathematical models, it was shown that while permalloy has approximately seven times the initial permeability and one third conductivity than permendur, permendur has a shorter switching time. However, through controlled pre-energized methods, permalloy can achieve improved switching times. The final reason given for a preference of permalloy is the better flux density and therefore is therefore better suited for holding open operations.

A model which can be represented by both an electrical and mechanical equivalent is described by Sung [21]. The design of the high speed solenoid utilized mathematical models to simulate response time, switching time, total force generated and maximum power needed to drive the system. The dynamic model used is a first order system

including the inductance 'L', reluctance 'R' for accounting for air gaps, and current draw 'i' as described in Equations 2-3 to 2-5.

$$\dot{x}_1 = x_2 \quad (2-3)$$

$$\dot{x}_2 = \frac{1}{M} [F_m - (R_v \cdot x_2) - (k \cdot x_1)] \quad (2-4)$$

$$\dot{x}_3 = \frac{1}{L(x_1)} [V(t) - x_3 \cdot R - x_3 \cdot \frac{dL(x_1)}{dx_1} \cdot x_2] \quad (2-5)$$

Where x_1 is the plunger position, $\frac{d}{dx_2}x_2$ is the plunger speed, and x_3 is the current.

$V(t)$ is represented in Equation 2-6. F_m , the force of magnetism is represented as a function of inductance 'L' but could also be represented by the number of coils 'N' and current 'i'. Reluctance 'R' is presented in Equations 2-7 and 2-8 as the air gaps shown in Figure 2-8 as g_1 to g_3 where 'R' is defined by Equation 2-7 as the length of the air gap divided by the area of the gap multiplied by the conductivity of air ' μ_0 '.

$$F_m(t) = \frac{1}{2} \cdot i(t)^2 \cdot \frac{d}{dx} L(x) \quad (2-6)$$

$$R = \frac{\text{Length}}{\mu_0 \cdot \text{Area}} \quad (2-7)$$

$$R(x) = R_1 + R_2 + R_3 \quad (2-8)$$

$$V(t) = i(t)R(x) + L(x) \cdot \frac{d}{dt} i(t) + i \cdot \frac{d}{dx} L(x) \cdot \frac{d}{dt} x \quad (2-9)$$

$$L(x) = N^2 / R(x) \quad (2-10)$$

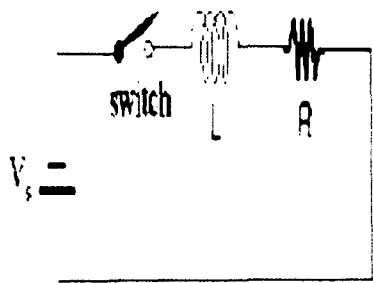


Figure 2-7a Electrical equivalent of solenoid

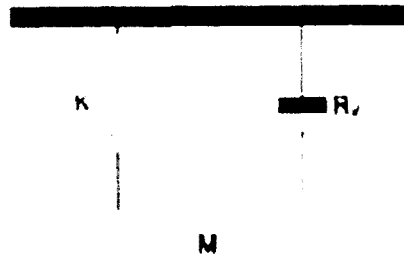


Figure 2-7b Mechanical equivalent of solenoid

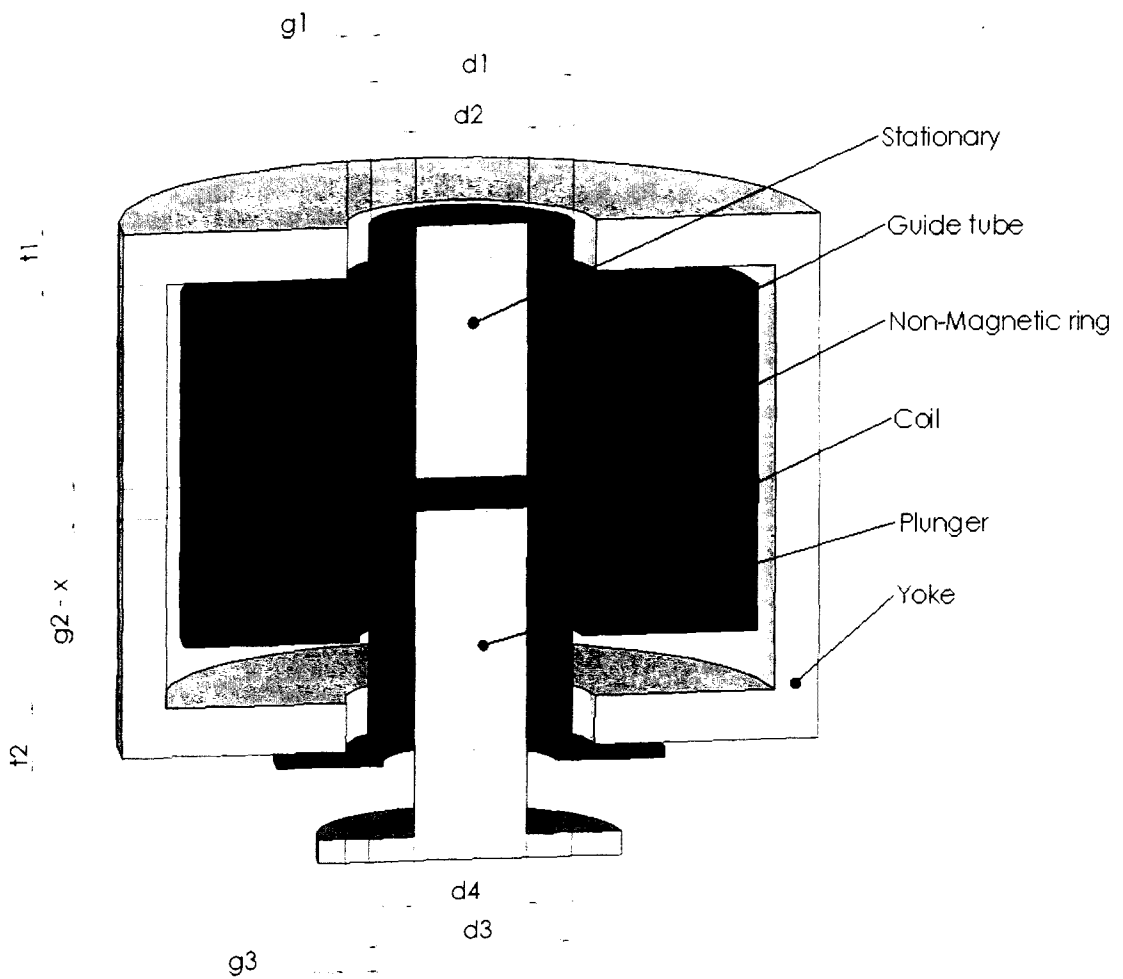


Figure 2-8 Section drawing of test solenoid

CHAPTER 3

DESIGN CRITERIA

Engine Modification

To modify an engine to operate on hydrogen, in the manner identified as direct in-cylinder injection, requires that the fueling system be capable of delivering fuel directly into the combustion chamber regardless of crank and valve position. For the case of the 425cc Polaris motor, a passage was milled into the cylinder head at the deck thus creating a direct passage between the injection unit and the combustion chamber whereas the design of the fuel injection system for the Ford V8 utilized the sparkplug passage. Both methods have advantages and disadvantages. Utilization of the sparkplug passage has three distinct advantages; 1) disassembly of the motor and machining of the cylinder head is eliminated, 2) a well-proven passage capable of withstanding combustion temperatures and pressures already exists, and 3) conversion of most ICEs to operate on hydrogen becomes more economically feasible. Milling a passage through to the combustion chamber has one distinct advantage namely, the injector is cheaper and easier to purchase and/ or manufacture.

The 1999 5.4 liter Ford V8 engine utilizes a cylinder head configuration called a *modular head* (Figure 3-1). The modular head configuration incorporates the camshaft into the head rather than in the block and most notably, the sparkplug passage is located between the valve cover and the intake manifold extending through the cylinder head to

the combustion chamber. This is significant when designing an injector/ sparkplug due to the long narrow passage which encapsulates the sparkplug (approximately 5 inches in length and a maximum of 0.890 inches in diameter). An in-depth look into the design of this injector/ sparkplug is addressed in Chapter 4. The Polaris engine, which also utilizes a long narrow passage for the sparkplug, was used to design and test the function of this particular injection system. For these reasons, the design of the sparkplug injector is such that it would fit these two particular motors as they would also represent a significant portion of vehicles.

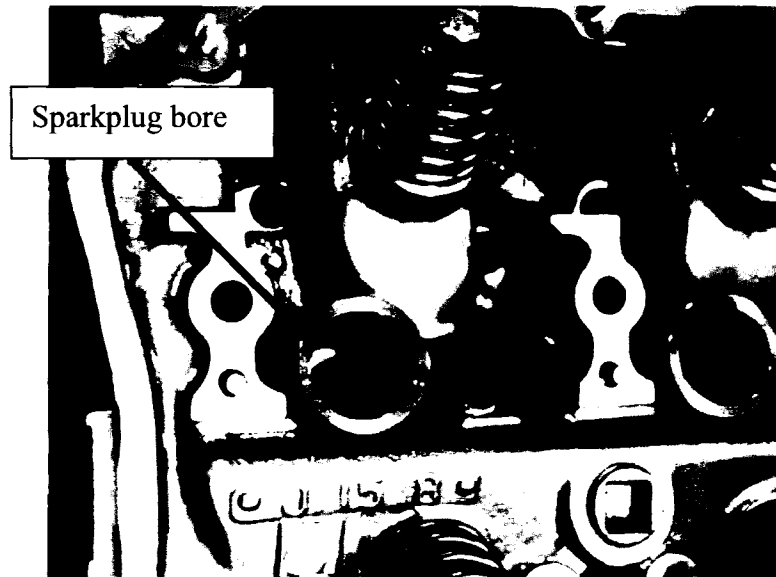


Figure 3-1 Ford modular head showing sparkplug bore extending through valve cover to center of combustion chamber.

Engine Simulations

Timing of critical events such as the injection and spark is the single most important factor when programming the computer system. The dynamics of the engine for the purpose of programming and designing components can be simplified to specifications

such as the effective compression ratio, bore, stroke, and swept volume. These specifications combined with input variables such as the AFR, fuel type, flame front propagation speed, ambient temperature, coolant temperature and various others can be used to simulate useful data such as emissions output, maximum torque and angle and various others. As mentioned previously, the flame front propagation speed is considerably faster than that of gasoline or other liquid fuels. For this reason, simulations were conducted to determine the most effective crank angle to ignite the fuel. While mathematically it is shown that the crank position, which corresponds to the highest torque is 29° ATDC; that is not to say that the fuel should be ignited at that exact point as well. Factors such as the combustion chamber pressure, temperature, air-to-fuel mixing pattern and density of the fuel directly affect the speed at which the flame front will propagate. To achieve maximum torque, it is necessary to have the maximum available pressure at the point corresponding to the optimum crank angle thus resulting in the maximum torque. For this reason simulations were conducted to determining angle of spark given engine conditions such as ambient temperature, desired AFR and engine speed.

Improved emissions of alternatively fueled vehicles tend to be a selling point. To demonstrate theoretical emissions values a simulation was conducted in MathCAD to determine production of NO_x , these values can then be correlated to actual emissions collected while load testing. The following set of data represents the results of one such simulation. The MathCAD file is found in the APPENDIX II. Figure 3-2 represents production of NO and varying AFR. It is noteworthy to draw attention to the increasing production of NO at am AFR around 45:1 (slightly lean) where production peaks after

which production tends to taper off. The tapering off is due to the decrease in combustion temperature due to less fuel being combusted. Figure 3-3 also demonstrates the trend for less production of emissions due to a decrease in temperature as the fuel mixture also goes lean (seen as an equivalence ratio less than 1).

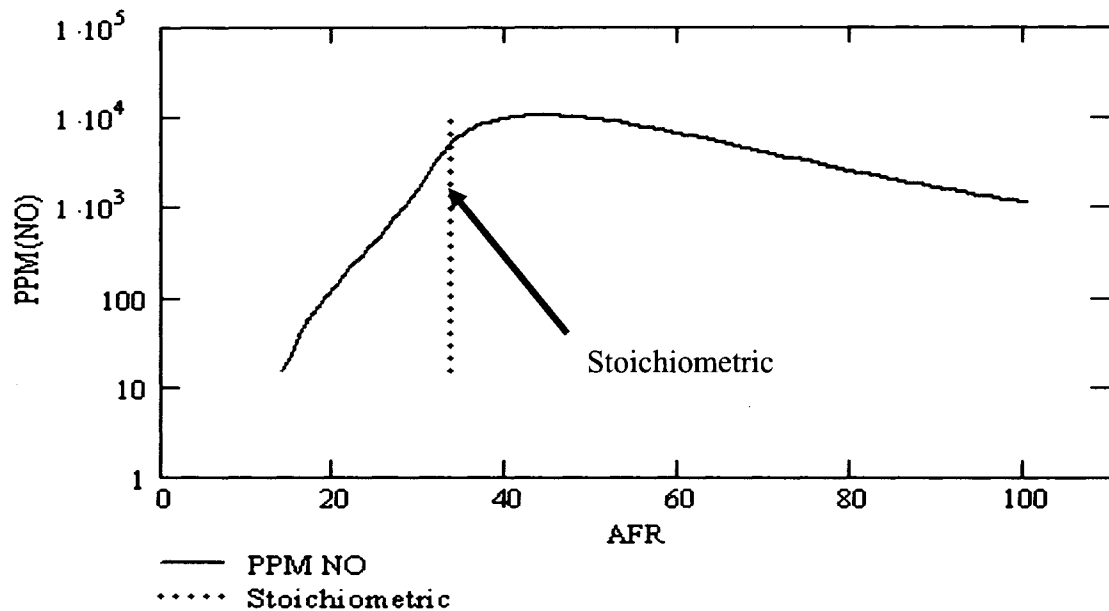


Figure 3-2 Simulation of emissions for a 425cc single cylinder engine

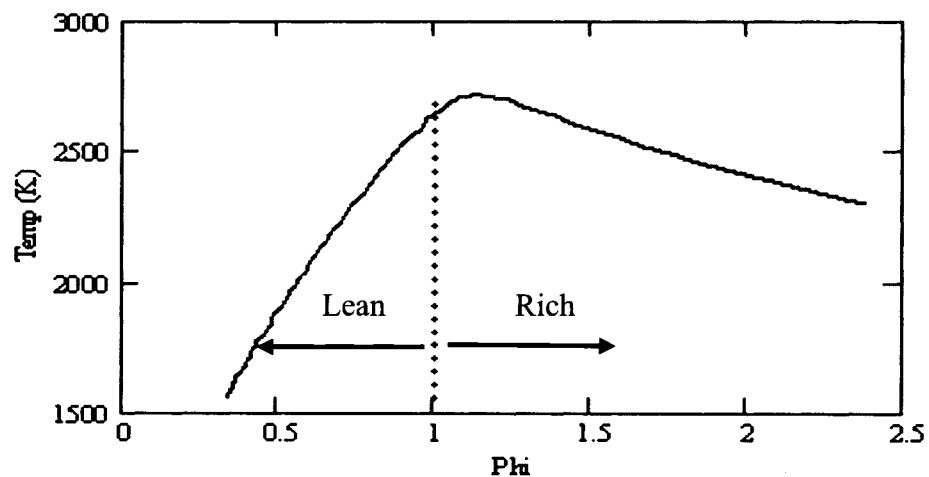


Figure 3-3 Simulation of adiabatic flame temperature for a 425cc single cylinder engine

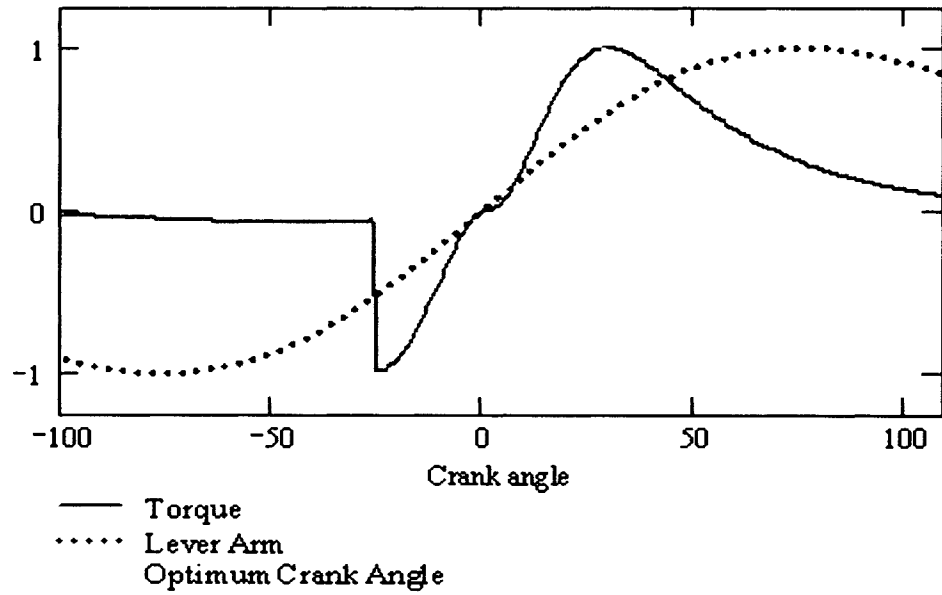


Figure 3-4 Torque profile of a single cylinder motor

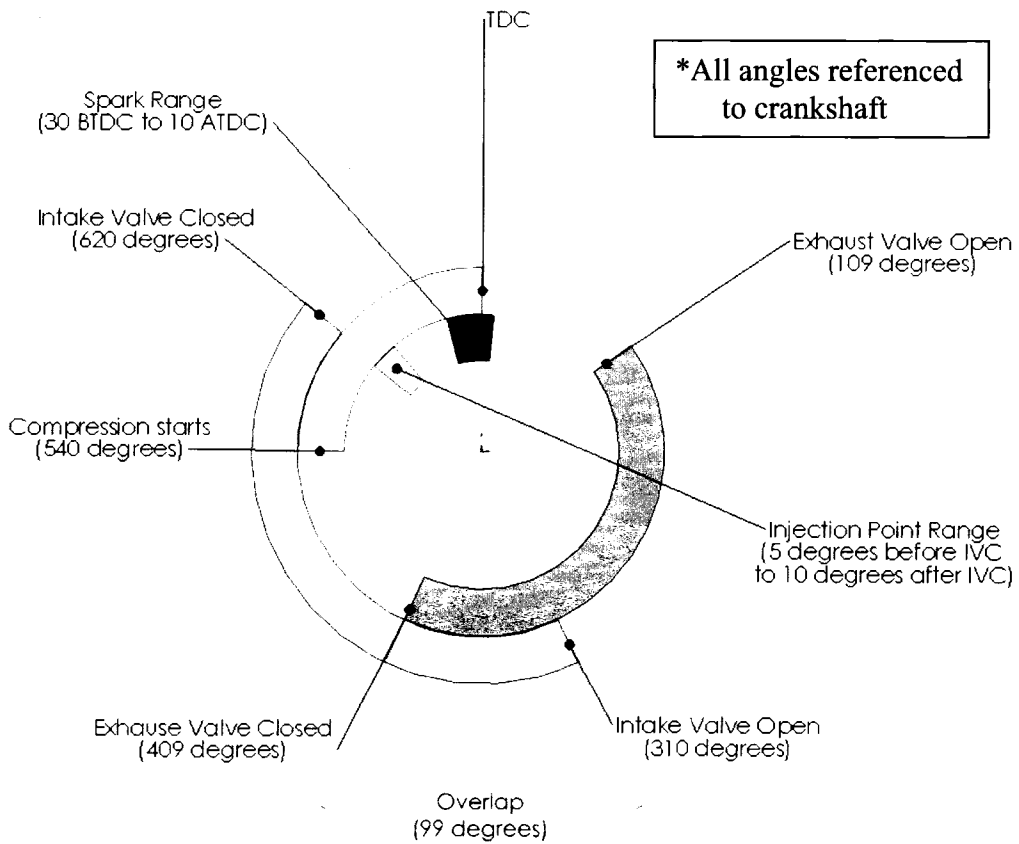


Figure 3-5 Engine timed events superimposed on camshaft cycle

Computer Modification

Conversion of the computer control system requires specific manipulation of the spark and fuel timing. Control of the Polaris engine required a new computer capable of controlling both the spark and fuel timing as required for direct injection. The entire computer system for the Polaris, including input sensors, programming and analysis software was supplied from KAM Products.

For the case of the Ford, it was necessary to reprogram the original computer (ECM). Software was purchased from SCT to completely reprogram the original Ford computer system. Simulations described previously for identifying optimum spark were used to design tables for spark vs. engine speed. As this is an inexact method refining via test driving and dynamometer testing will also need to be performed. For safe operation of the Ford ECM an injector with an internal resistance of 10 to 16 ohms is necessary. For proper control over the solenoid designed for the injection a higher current draw than what the ECM is capable of is necessary. For this reason, a standalone driver board with solid-state relays capable of handling voltages up to 48 VDC and 15 amps was placed in series to the injector output wiring scheme.

Table 3-1 Typical timing events for hydrogen engine

Computer controlled timing events		
Injection	For all RPMs	640 ATDC
	Startup	20 ATDC
	Idle	22 BTDC
Spark Timing	MAP = 20 inHg	5 BTDC
	MAP = 30 inHg	4 ATDC

Spark Modifications

The flame front propagation for hydrogen is 5 times faster than that of gasoline [16] and therefore special care should be given to the spark timing of an engine operating on hydrogen fuel. Spark for an engine fueled by gasoline or equivalent fuel is initiated at a crank angle of 10° to 20° BTDC at idle, and up to 37° BTDC at max RPM and load. Because of the nearly instantaneous pressure increase associated with hydrogen [24], spark for a hydrogen fueled engine should be initiated at or later than 0° BTDC and will be shown experimentally to occur at 10° ATDC as a minimum angle. Failure to compensate for the flame speed will result in the engine either rotating backwards or a backfire through the intake system. For the case of the Polaris engine conversion, the initial spark to start the engine occurs at 20° ATDC.

Experimentally it has been shown that typical flame speed for combustion of hydrogen in air, under stoichiometric and standard conditions, is approximately 13 meters per second. In a combustion chamber of the size found in the Polaris, this corresponds to a typical burn time of 3.41 ms. As an example for an engine at a speed of speed 4500 RPM the crankshaft is rotating at 27° per ms, the fuel must be ignited no more than 92° prior to the optimum crank position (angle resulting in the highest torque for the pressure generated from the burning fuel). This means that if the crank position for optimum power is at 72° ATDC, the spark can not be initiated before 20° BTDC otherwise peak pressure and complete burning of the fuel occurs before the optimum crank position thus resulting in a loss of power output.

Computer simulations were conducted to determine the optimum crank angle for a particular engine speed that the spark should occur. Variables entered into the simulation

are the flame propagation speeds [24] and geometry of the engine including displacement, stroke, and connecting rod length. The following set of data was derived from this simulation shows optimum spark resulting in the highest possible torque.

Table 3-2 Optimized ignition angle for Polaris motor

RPM	Crank Speed (deg/ ms)	Complete Burn (degrees)	Calc. Flame Speed		Optimized Ign. Angle (BTDC)
			(ft/sec)	(ms)	
1500	9	37	5.07	3.8	5
2000	12	37	6.22	3.1	8
2500	15	38	7.57	2.5	9
3000	18	39	8.85	2.2	10
3500	21	41	9.82	2.0	12
4000	24	42	10.95	1.8	13
4500	27	43	12.03	1.6	14

Fuel Modifications

Typical aspirated or port injection motors will need for the fuel to be delivered while the intake valve is open. For the purpose of delivering fuel directly into the cylinder, there is no need to deliver fuel when the intake valve is open. Delivery of fuel when the intake valve is open will displace as much as 30% by mass of air, at stoichiometric conditions thus lowering power output and volumetric efficiency. Based on the geometry of the engine, optimum crankshaft leverage occurs around 80° ATDC; however, as demonstrated in Figure 3-4, optimum pressure resulting in the highest torque occurs around 29° ATDC. Regardless of fuel pressure/ fuel delivery speed, there should be significant levels of hydrogen in the combustion chamber at the time the spark needs to be initiated, and completely fueled at such time the exhaust valve is opened.

Injector Design

The related timing issues for the injection system, as it pertains to the turn-on signal and duration are elements designed into the control system. The injector design should meet specific requirements such that the control system is capable of controlling the functions of the injector. For example, the type of solenoid valve (power requirements and response time) and overall length of the injector play important roles when determining the exact point at which the control system can/ should turn the injector on.

The injector, as defined for this report, is strictly referred to as a device capable of delivering fuel in a manner consistent with the requirements needed to sustain combustion in an internal combustion engine. This device contains, as a complete unit, a solenoid valve and check valve. It is not required that the unit be a single device containing all parts, but rather the sum of the parts comprise the injector.

Specific requirements of the injector are the solenoid be thermally and electrically protected, be fully responsive up to 40 Hz, and deliver a mass flow rate as low as 0.1 lb_m/hr and at least 2 lb_m/hr. A flow rate of 0.1 lb_m/hr will ensure adequate control of the idle and a flow rate of 2 lb_m/hr will ensure enough fuel is delivered for full power output of the cylinder.

CHAPTER 4

COMPONENT DESIGN

Polaris Engine

Various components were both developed as well as purchased such that when combined form a high pressure injector for use as a direct injection unit. A solenoid capable of withstanding inlet pressures up to 1500 psig and a media temperature of 0 to 150 °F was purchased from Peter Paul Electronics Co. Inc. A check valve capable of handling peak combustion pressures and extreme temperatures was developed for the purpose of protecting the fuel solenoid from exposure to excessive temperatures and pressures.

Check Valve

The main purpose of the check valve is to protect the fuel solenoid from exposure to flame, excessive temperature, high combustion pressure during ignition, pre-ignition and backfires as well as to maintain the correct compression ratio. The check valve functions by keeping backflow negligible and opening when the pressure differential is sufficient enough to overcome the spring force and combustion chamber pressure. During the compression stroke, while fuel is added to the combustion chamber, oxygen can be compressed into the fuel nozzle. If adequate protection against temperature, flame, pressure and backflow is not utilized and spontaneous combustion occurs, a flame can freely travel up the fuel line to the solenoid, thus rendering the solenoid inoperable.

Spontaneous combustion, for hydrogen, can occur at temperatures as low as 1050 °F. Exhaust temperatures under heavy loads can average around 1800 °F and an instantaneous combustion temperature/ adiabatic flame temperature can be calculated as high as 4000 °F. A good rule of thumb for minimizing the chances of a spontaneous combustion (oftentimes referred to as a pre-ignition) is to minimize the combustion chamber and/ or coolant temperature, using cold sparkplugs and by removing hot spots such sharp edges within the combustion chamber or lowering the thermostat temperature rating. A good approximation for determining the maximum allowable pre-compression cylinder temperature is to treat the compression stroke as a polytropic compression process as described in Equation 4-1 where 'T' is defined as the auto-ignition temperature and 'To' is the pre-compression temperature, 'CR' is the compression ratio of the engine and 'k' represents the ratio specific heats for the air/fuel mixture. Table 4-2 summarizes various methods of injection for hydrogen and compressed natural gas and the corresponding pre-compression combustion chamber temperatures based on Equation 4-1.

$$T_o = \frac{T}{CR^{k-1}} \quad (4-1)$$

Therefore, it is obvious that hydrogen gas as a fuel has a high probability to pre-ignite due to temperature. Furthermore, the walls of the combustion chamber are cooled by the engine coolant (as in the case of this motor) and thereby provide a means to heat the air prior to compression and injection of the hydrogen gas. It is for this reason that the coolant temperature must be minimized in order that ignition of the hydrogen gas occurs

due to the spark alone and not the temperature. Experiments on Polaris motor have showed that operation with a coolant temperature above 170 °F promotes pre-ignition.

Table 4-1 Combustion chamber temperature due to polytropic compression

Fuel	k of mix	Auto-Ignition Temp (°F)	Max temp prior to compression (°F)
H2 (Port)	1.41	1050	148
H2 (Direct)	1.40	1050	161
CNG (Port)	1.16	1040	582

A more accurate method for approximating the temperature of the gas mixture, immediately after the compression stroke, is to account for both the temperature drop due to the expanding hydrogen injected into the combustion chamber as well as to use the effective compression ratio rather than the published compression ratio. The compression ratio is by definition the entire volume of the combustion chamber including the cylinder head volume at BDC divided by the minimum volume at TDC. This calculation however does not account for the closing of the intake valve. The intake valve of a typical engine can close up to 100° after the compression stroke has initiated (100° ABDC). Therefore the pressure within the combustion chamber will not begin to increase until after the intake valve has nearly closed which in effect has a tendency to decrease the compression ratio. For example, the Polaris engine has a published compression ratio of 9.2:1, however when accounting for the closing of the intake valve, the effective compression ratio is decreased to 6.3:1.

Seat and plunger material selection was critical for the development of the check valve. Typical application for the check valve requires the plunger and assembly withstand cyclic loading up to 6000 psi at a frequency of 45 Hz (5500 RPM). Table 4-2 represents all the materials used during testing and the results including predicted failure time. The pressure-differential operated check valve was developed to meet the above operational requirements, material fatigue suitability, as well as the requirements presented by the use of hydrogen (galling from no lubrication and high moisture content at the point of ignition). Figure 4-13 shows the schematic cutaway of the high pressure check valve. The design of the check valve took into account the possibility that any part may need to be changed especially during the testing portion of the project and therefore all parts are standardized by dimensions or is able to be purchased.

As part of the design process, it was necessary to determine materials that would function well in an environment in which the temperature is cyclic in nature, may experience large impact forces, and is wear resistant with self lubrication properties. Five materials were chosen as possible candidates to comprise the check valve assembly. Alloy 901 contains between 40% to 45% nickel which under impact conditions has a tendency to work harden thus making the sealing surface impervious to wear. Bronze materials 673 is a manganese based brass well suited for high pressure and cyclic temperatures. This material is commonly used in race engines for the valve seats of the exhaust valve. Bronze material 630 is similar to the 673 in function. The material is more commonly referred to as nickel aluminum bronze. The material referred to as C27 Bronze is a high ferrous bronze well suited for high temperatures and pressures. The exact material composition is unknown however, C27 refers to the hardness on the

Rockwell C scale. Finally, 300 series stainless steels were tested. Due to the fine grain lattice structure, good hydrogen embrittlement properties and the high quality finish capable of being machined, this material is well suited for high temperature fluctuations. Table 4-2 describes tests performed on the check valve assembly at an engine speed between 2500 and 4000 RPM. While alloy 901 performed extremely well, manufacturing of a check valve assembly would require extensive work. Alloy 901 is excellent for impact resistance, however, lacks the self lubricating properties required. The final choice was to use a 316 SS plunger with the C27 Bronze as the seat material.

To insure that the working pressure is within the stress limit of the housing hoop stress and thermal expansions limits calculations were made at critical points along the housing. The critical points of interested, as depicted in the section view of the check valve, are as follows 1) inlet connector wall thickness, 2) snap-ring grove, and 3) threads. Equations 4-2 and 4-3 represent hoop stress for thin and thick walled tubes respectively. Where 'p' is the pressure, 'r' is the inner radius, and 't' is the wall thickness as depicted in Figure 4-1.

$$\sigma_h = \frac{p \cdot r}{t} \quad (4-2)$$

$$\sigma_h = p \cdot \left(\frac{L^2 + 1}{L^2 - 1} \right) \quad \text{where} \quad L = \frac{OD}{ID} \quad (4-3)$$

$$\epsilon_T = \alpha \cdot \Delta T \cdot L \quad (4-4)$$

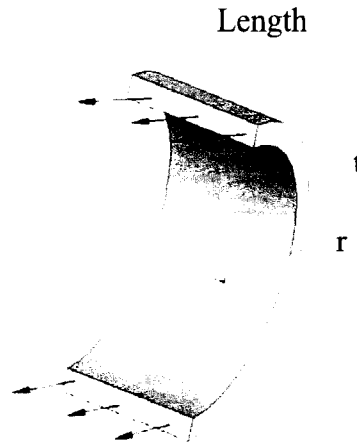


Figure 4-1 Stress in the hoop direction for a cylinder

Equations 4-5 and 4-6 represent calculations for torque applied on threads and the maximum bearing stress on a thread wherein 'f' represents the friction of the threads, 'd_m' is the mean diameter, 'f_c' is the friction of the collet/ hardened seat, 'α_n' represents half the thread angle, 'd_c' is the diameter of the hardened seat, and 'L' is the lead of the thread.

$$\text{Torque} = \frac{\text{Load} \cdot d_m}{2} \cdot \frac{f \cdot \pi \cdot d_m + L \cdot \cos(\alpha_n)}{\pi \cdot d_m \cdot \cos(\alpha_n) - f \cdot L} + \frac{\text{Load} \cdot f_c \cdot d_c}{2} \quad (4-5)$$

$$\sigma_{\text{Thread}} = \frac{4 \cdot \text{Load}}{\pi (d^2 - d_1^2)} \cdot \frac{\text{pitch}}{t} \quad (4-6)$$

Table 4-3 Safety factor of critical points of Polaris check valve

Critical Point	Hoop Stress (PSI)	Bearing Stress (PSI)	Temperature Stress (PSI)	S.F. @ 110% of working pressure
1) Gas connector	2274	NA		2.99
2) Snap-ring	NA	128	9369	3.66
3) Threads	NA	834		3.41

Testing of the check valve to determine appropriate material selection consisted of construction setups for runs identified in Appendix I, Table AI-3. Each run consisted of operating the engine at 75% to 100% of full load for varying times between 2 hours and 6 hours with measurements for impact fatigues occurring every 30 minutes. Data recorded were as follows: initial depth as identified in Figure 4-2, maximum and minimum temperature at the base of check valve assembly, and the final depth as identified in Figure 4-2. Determination of material selection was chosen based on machinability, average operating temperature (indication of the sealing quality-lower temperature implies a better seal), and projected longevity based on the acquired measurements found in Table A1-3.

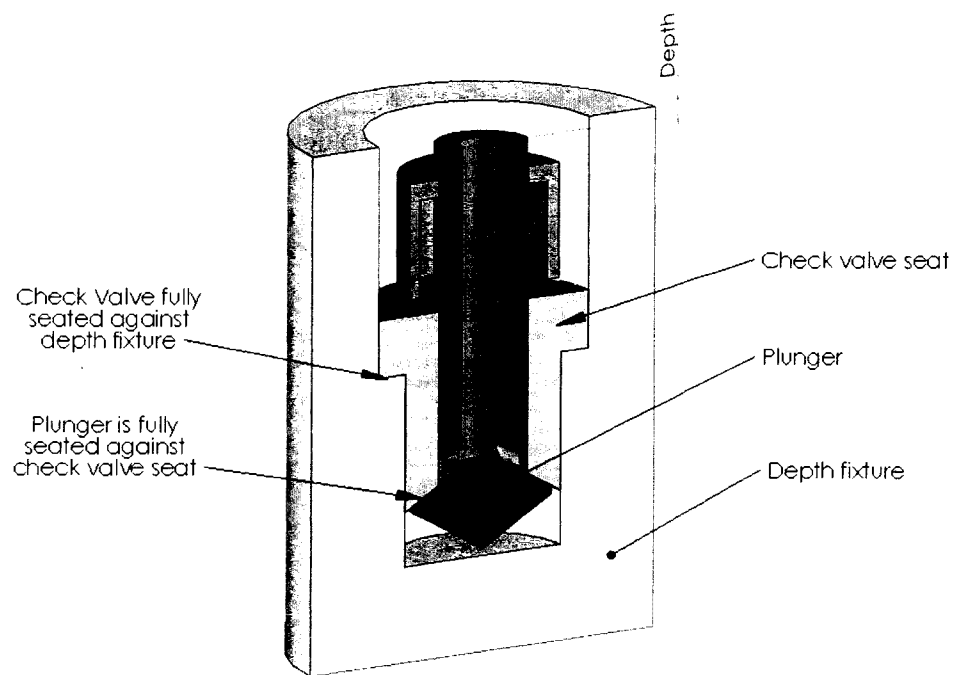


Figure 4-2 Measurement for check valve impact fatigue diagram

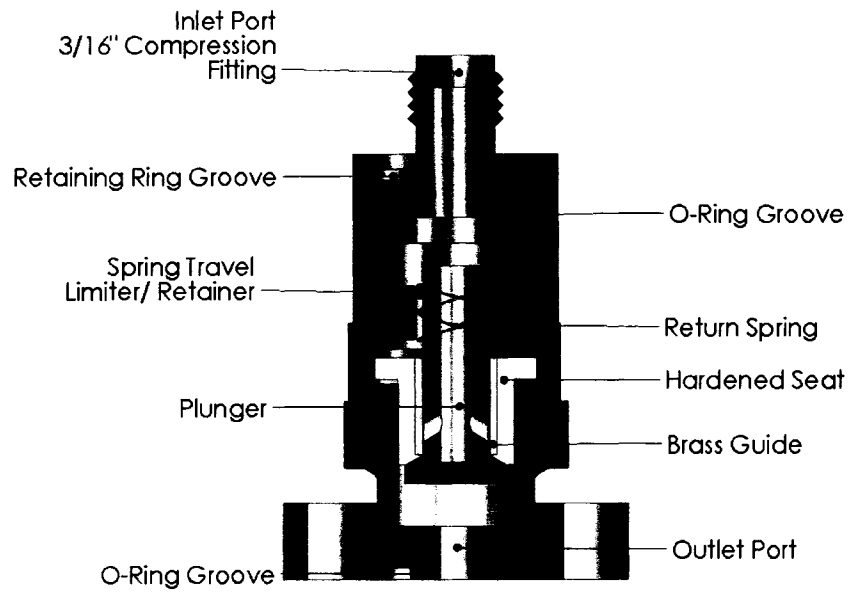


Figure 4-3 Section view of Polaris check valve

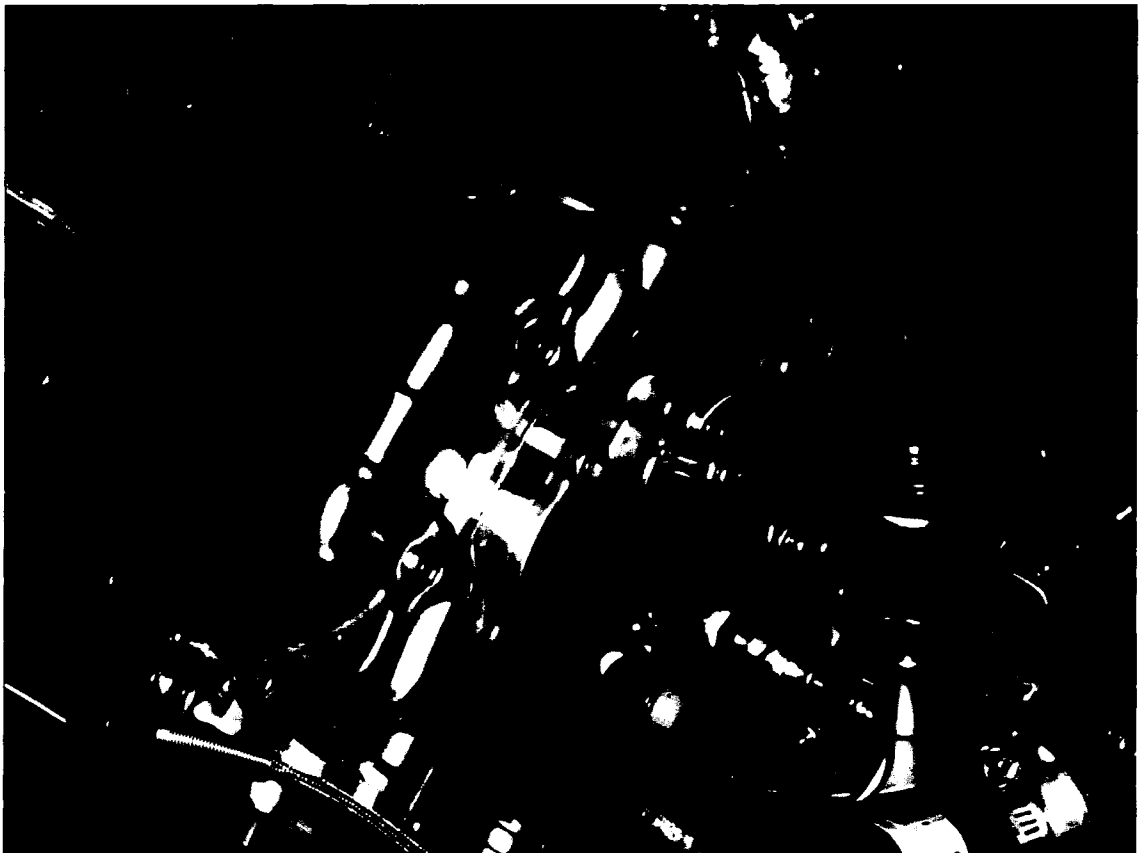


Figure 4-4 Polaris engine with fueling modifications

Timing Components

For simplicity, all moving engine component angular positions are referenced with respect to the crankshaft. A four-stroke motor can be identified by four operations (intake, compression, combustion, and exhaust) completed every two crankshaft revolutions. Valves are opened and closed in sequence to make these four operations possible. For the camshaft to operate this sequence of movements, it is necessary that the camshaft rotate at half the speed of the crankshaft, thus there is one unique position for the camshaft and crankshaft such that the piston is considered at top-dead-center (TDC).



Figure 4-5 Camshaft timing components for Polaris motor

Two dual differential Hall-effect sensors are used to determine the position of the piston with respect to TDC (farthest position of piston from the center of the crank shaft

on the compression stroke); one to verify the camshaft position (Figure 4-5) and one referencing the flywheel (Figure 4-6) which defines the instantaneous angle of the crankshaft. When combined the computer is able to determine both the exact position of the crankshaft was well which of the 4 cycles the engine is currently on.



Figure 4-6 Crankshaft timing components for Polaris motor

Ford Engine

High Pressure Injector

To individually test and evaluate the design of the sparkplug injector, the Polaris motor was used in lieu of the Ford engine for the simplicity of a single cylinder as well as a similar sparkplug passage. The concept behind incorporating the sparkplug and injector was to utilize an existing passage that is directly linked to the combustion chamber. The design of the injector consists of a ceramic insulator spanning the entire length of the injector through which the electrode carrying the high voltage needed for the spark as

well as the high pressure hydrogen gas are electrically insulated from the rest of the engine. A section view of the injector is found in Figure 4-7. The internal check valve is identical in purpose to that of the Polaris injection unit which is to protect the internal components from excessive pressure and temperature as well as to maintain the compression ratio.

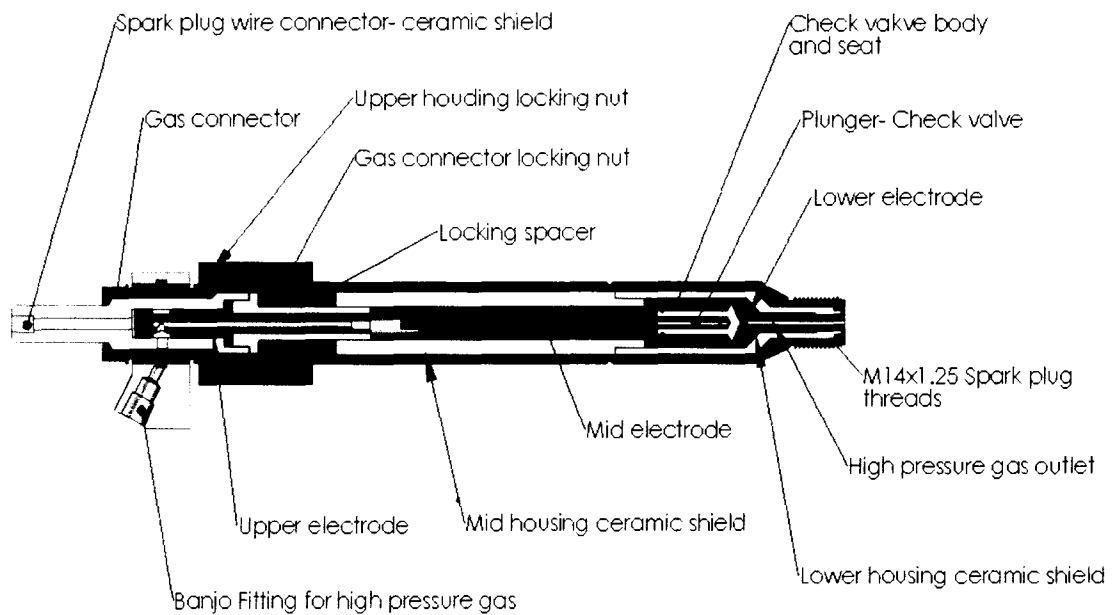


Figure 4-7 Section view of sparkplug injector with external solenoid valve

The sparkplug injector is broken into three parts; 1) the electrodes and check valve, 2) the high pressure solenoid valve and 3) the gas inlet and sparkplug wire connector. The function of the solenoid valve is to meter the mass flow of hydrogen into the combustion chamber. For testing purposes, the sparkplug injector was designed with a detached high pressure solenoid valve attached to the injector via a stainless steel tube. For the purposes of testing just the solenoid valve, separate test fixtures were designed specifically for the solenoid test and therefore did not include any electrodes or ceramic insulators. The

design of the injector housing incorporates the capability to operate the injector with or without the internal solenoid valve.

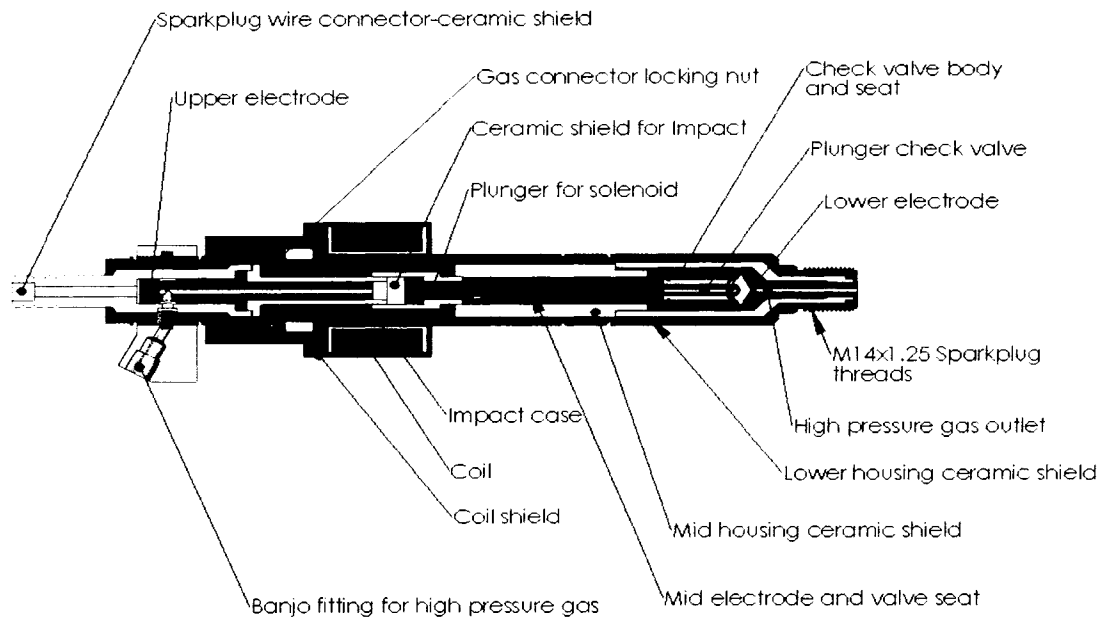


Figure 4-8 Section view of sparkplug injector test module

Design of the injector considered various stresses from the internal high pressure gas, temperature and contact of materials with different thermal expansion coefficients. Table 4-3 summarizes the factor of safeties for stress at each critical point. The critical points of most interest, as depicted in figures 4-10 and 4-11, are: 1) banjo fitting gas ring, 2) section where ceramic is sandwiched between stainless steel, 3) wall of housing and 4) ceramic sandwich at tip of injector. Equations 4-2 through 4-4 were again used to make these calculations.

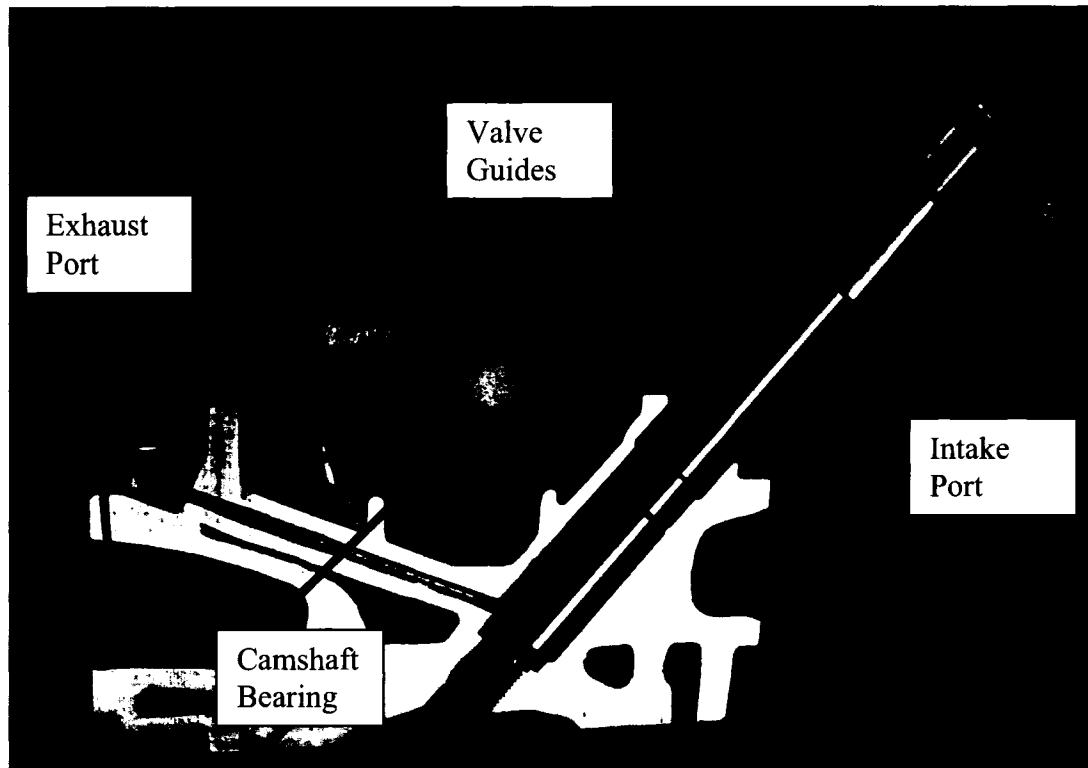


Figure 4-9 Polaris cylinder head cutaway

Table 4-4 Safety factor of critical point for sparkplug injector

Critical Point	Hoop Stress (PSI)	Temperature Stress (PSI)	S.F. @ 110% of working pressure
1) Banjo gas ring	14000	NA	2.37
3) Wall of housing	5471	10500	2.18

Critical Points 2 and 4 require more calculations than can be simplified in the above table. Contact between materials (if existent) must be considered as this will contribute to the strain in each part. For the case of critical point 4, the outer portion of the housing is contained within the cylinder head and is considered to be stable at all operating temperatures and pressures. Furthermore, there is no initial contact between the inner electrode and the ceramic, however due to the limits of machine ability, contact is

assumed for this set of calculations to make the scenario more realistic. As an example of these two scenarios, if no contact is assumed, the factor of safety is roughly 9.11 whereas if initial contact is assumed, stresses are transmitted via thermal expansion and expansion due to pressure. The factor of safety for this scenario is calculated to be 2.91 at 110% of working pressure. The same situation applied for critical point #2, if no contact is assumed between parts (as designed) the factor of safety is 6.73, however, if a more realistic scenario is assumed where all parts are initially in contact, the factor of safety drops to 1.8.

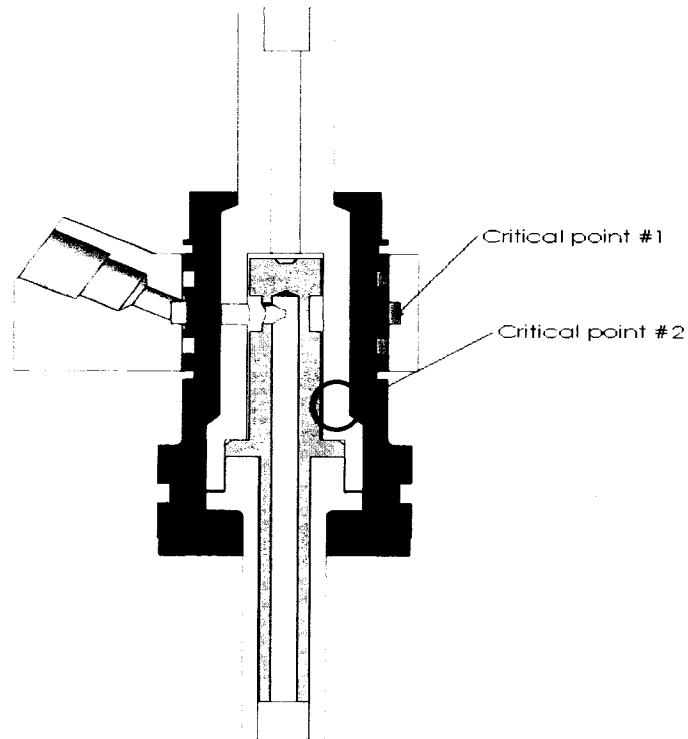


Figure 4-10 Critical point on gas coupler assembly

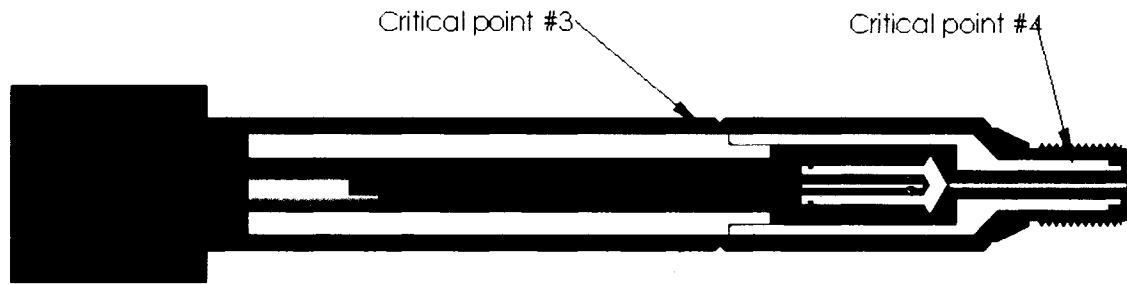


Figure 4-11 Critical points on housing

Design of Internal Valve

The design of a solenoid valve suitable for use with hydrogen was broken into two distinct sections: 1) a coil to operate the mechanical sealing mechanism and 2) the sealing mechanism or valve. Because this injector will also function as a sparkplug, electrical insulation of the coil is of utmost importance. With a metallic core running through the center of the coil (electrode for the spark) the high voltage of the spark will induce a voltage through the solenoid. This high voltage can be electrically isolated from the computer control via use of a diode in the driver control mentioned previously. If however, the coil is in close proximity to the electrode with little to no electrical insulation, a high voltage from the electrode will seek the shortest path to ground thus shorting the coil wires and rendering the solenoid inoperable. For protection of the coil and to insulate the entire span of the electrode from an internal short, a ceramic shield also spanning the entire length of the injector was designed of the same material as used in a typical sparkplug; alumina (Al_2O_3). The material chosen for this injector is 99.6% pure with an electrical strength of 500 volts per mill. The high purity and consequently high electrical strength is necessary due to the thickness of various portions of the ceramic and an expected voltage of up to 20,000 volts.

Design of the coil comes from basic concepts of electromagnetism. Equation 4-2 describes the magnetomotive force 'F_m' as the number of turns times the current 'i' and Equation 4-3 describes the force exerted to an iron core having a cross-sectional area of 'A' and the total gap between ferrous parts that the magnetic field follows as 'g'.

$$F_m = N \cdot i \quad (4-2)$$

$$F = \frac{F_m^2 \cdot \mu_0 \cdot A}{2 \cdot g^2} \quad (4-3)$$

$$B = \frac{\mu \cdot N \cdot i}{L} \quad (4-4)$$

To verify working conditions at elevated temperatures it is necessary to determine the change in resistance of the windings of the coil. Equation 4-5 represents, in °F, the change in resistance of the coil as referenced to standard conditions. 'R_o' represents the resistance of the wire at 'T_a', where 'T_a' is the ambient temperature.

$$R = \frac{R_o}{1 - 0.00393 \frac{5}{9} (T_f - T_a)} \quad (4-5)$$

Two variations of the solenoid valve were designed and tested for suitability including ease of access to failed parts, longevity and adequate electromagnetic force to open valve at 110% of working pressure. The first valve assembly tested was an internal solenoid. Figure 4-12a is a section view of the test apparatus used for testing of the internal solenoid. The second solenoid setup consisted of an external coil with the valve moments internal as shown in Figure 4-13a. Due to the confining nature of the sparkplug passage and limitations of the plunger design (large cross section and weight), it was

determined through medium pressure tests (up to 600 psig) the solenoid design as configured in Figure 4-12 can not produce the desired electromagnetic force required.

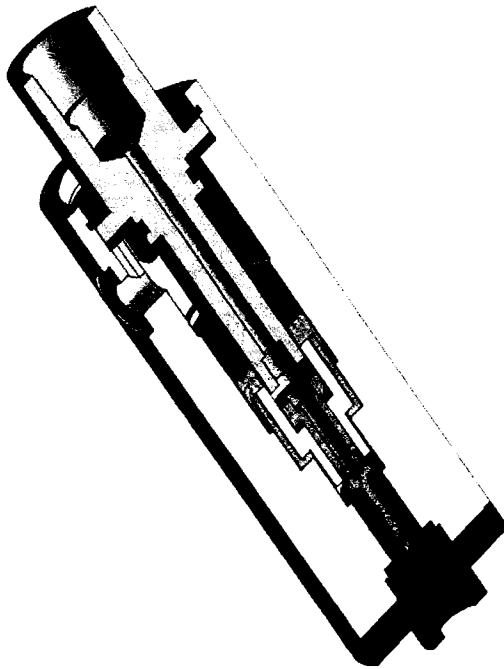


Figure 4-12a Section view of test fixture for internal pressure valve.



Figure 4-12b Test fixture for internal high pressure valve

To overcome the dimensional limitations, the injector body was lengthened and an external coil was designed to operate the internal valve components. This design had two distinctive advantages over the internal coil scheme; 1) A larger coil capable of producing adequate electromagnetic force was achievable and 2) sealing issues arising from designing a pressurized housing with coil leads extending through the housing were eliminated.

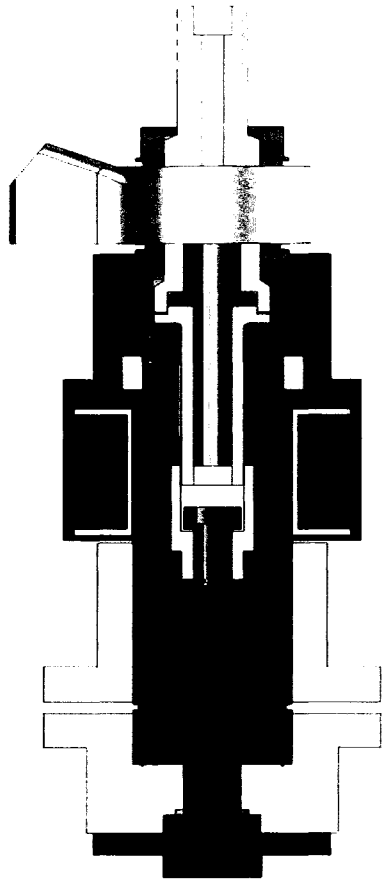


Figure 4-13a Section view of external coil, high pressure valve

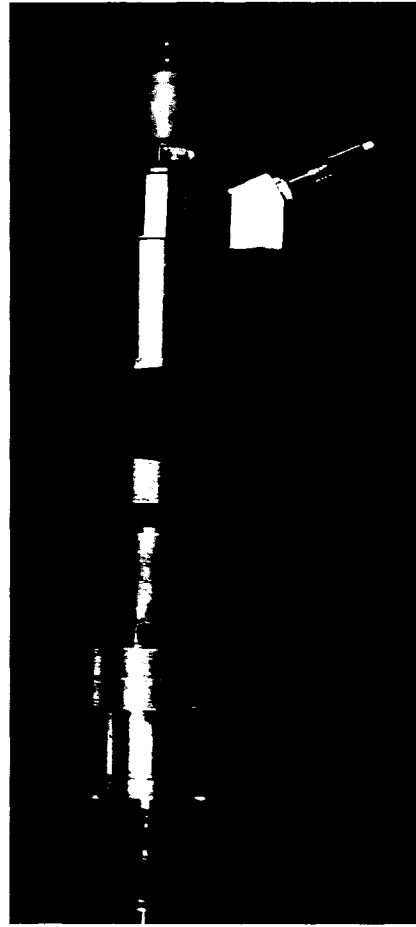


Figure 4-13b Test fixture for external coil, high pressure valve

CHAPTER 5

VEHICLE CONVERSION

The conversion of the vehicles consisted of three distinct tasks; 1) installation of the plumbing and necessary mounting hardware, regulators, valves, tanks, and data acquisition, 2) conversion of the engine including injector(s), sensors and sensor brackets, and throttle body, 3) programming of the ECM.

Each type of vehicle is unique in placement of key components such as the tanks, regulators, etc, but all are similar in the general tasks. The Polaris vehicle required a complete computer and harness along with necessary sensors, injection unit, etc. whereas the Ford vehicle required reprogramming of the original ECM and installation of the injection system, plumbing and fuel storage tanks.

Polaris Conversion

Conversion of this vehicle consisted of removal of the cylinder head for milling, installation of the check valve onto the milled head, fabrication of the throttle body, vacuum chamber, and mound for the injector solenoid. Milling of the cylinder head consisted of a small passage, measuring 0.062" ID x 1.5" in length, which connected the combustion chamber to the check valve/injection unit. Mounting of the check valve assemble was carried out by milling a flat portion of the cylinder head unto which the check valve unit is bolted in place. An air tight seal is made between the mounting surface and the check valve through use of a high temperature o-ring and bolts. The

geometry of the cylinder head and relations between the injection point, sparkplug and valves are depicted in Figure 5-1.

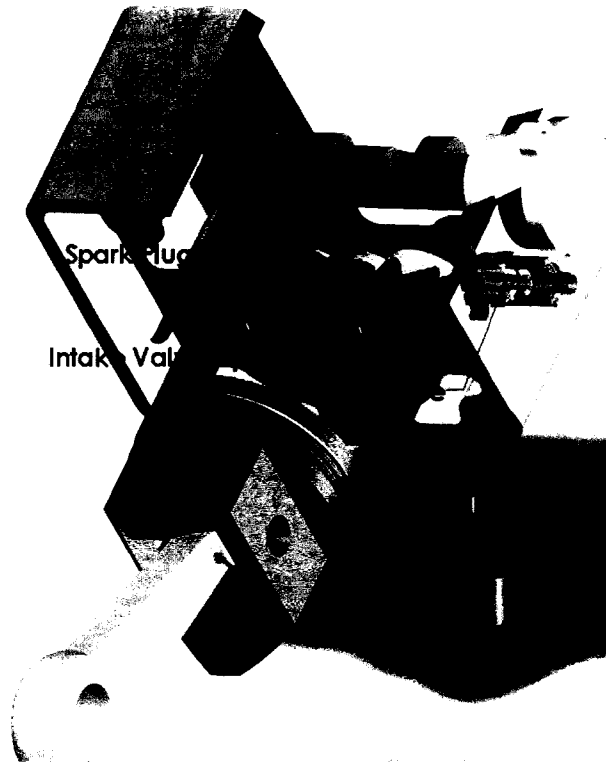


Figure 5-1 Polaris vehicle final conversion

Placement of the fuel passage is critical in achieving homogeneous and quick mixing of the air and fuel as well as ensuring a supported flame front. As demonstrated in the 3-D representation of the cylinder head configuration, the fuel passage is directed towards the sparkplug slightly towards the intake valve and slightly downward. This specific orientation was specified to ensure a rotating cloud of homogeneous mixture of fuel and air. Position of the check valve assembly in relationship to the throttle body and various sensors attached to the engine are depicted in Figure 5-2.

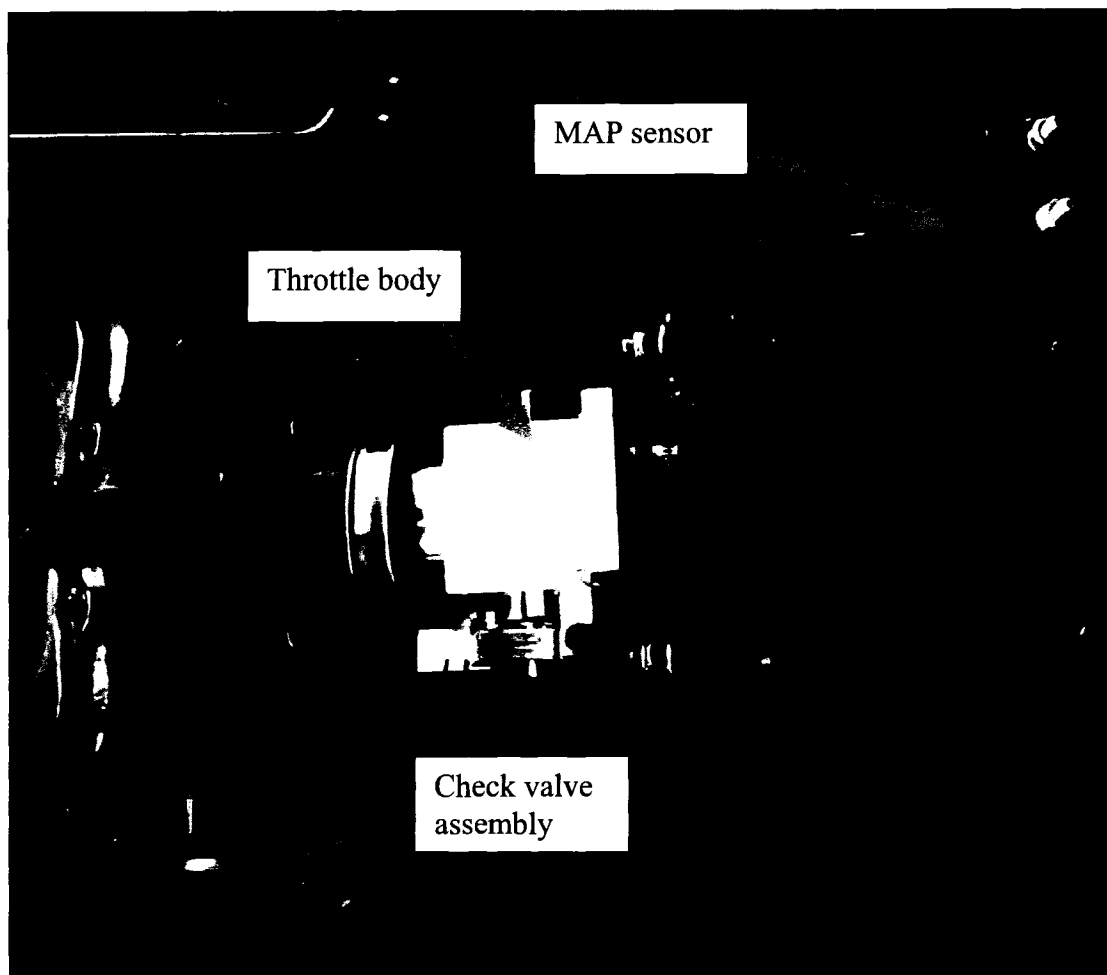


Figure 5-2 Engine compartment of Polaris engine

Electrical System

Electrical system conversions essentially consisted placement of additional circuits to accommodate new hardware such as relay boxes and sensors. The electrical system on the Polaris vehicle is unaltered with the exception of the addition of the relay box (Figure 5-4). Contained within the relay box is an automatic shutdown sequencer, relays for individual systems such as the injector control, fuel tank solenoids and secondary driver systems indicating fuel pressure. The shutdown sequencer is engaged when the ignition switch is turned to the off position at which time the sequencer will immediately turn off the tank solenoid. However the computer electronics will remain functioning for an

additional 5 seconds. The additional time will ensure the engine continues to operate thus consuming the remaining fuel from the fuel lines at which point the remaining fuel is not sufficient to maintain operation of the engine. This will occur when the fuel mixture in the combustion chamber is below the flammability limits of hydrogen.

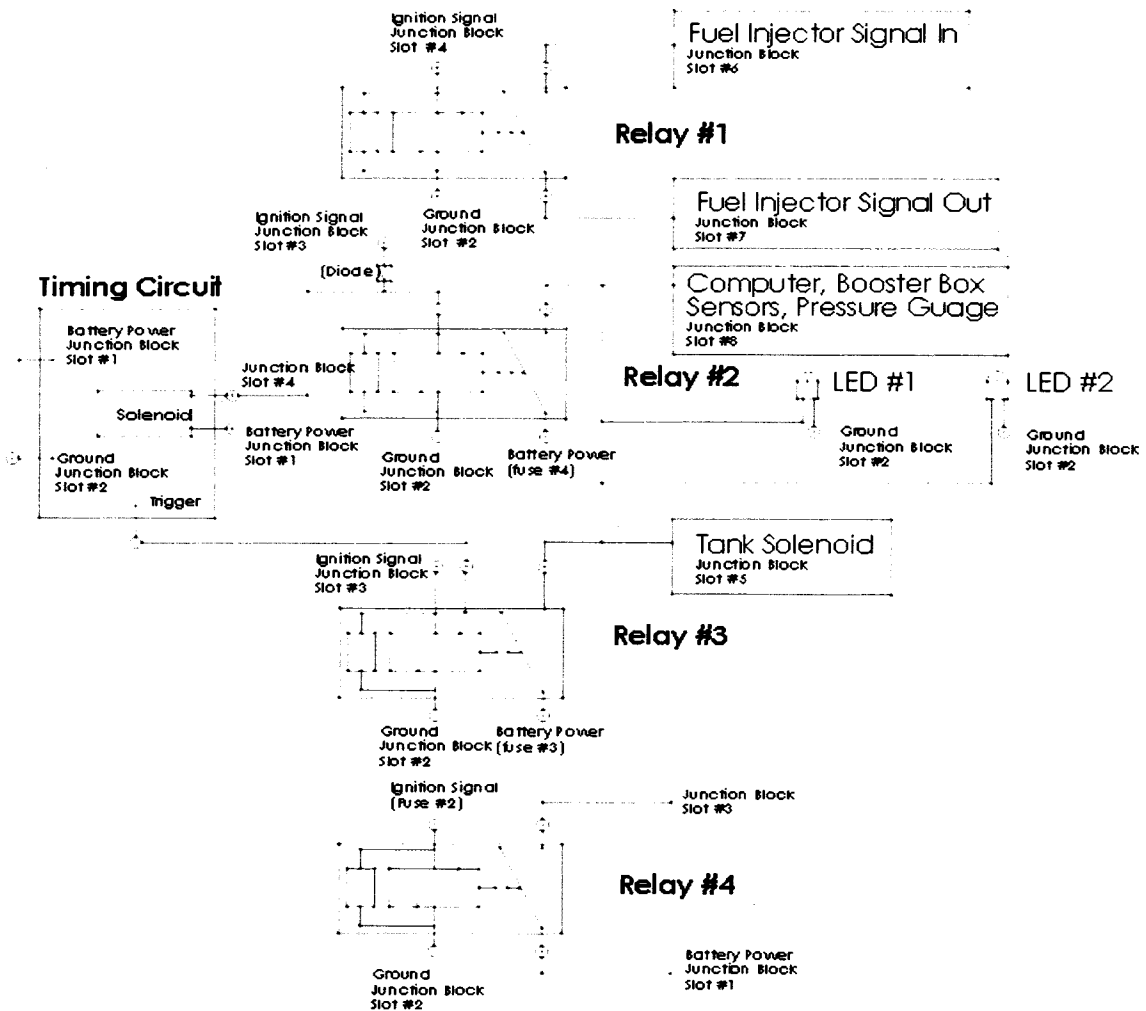


Figure 5-3 Wiring scheme of Polaris relay box

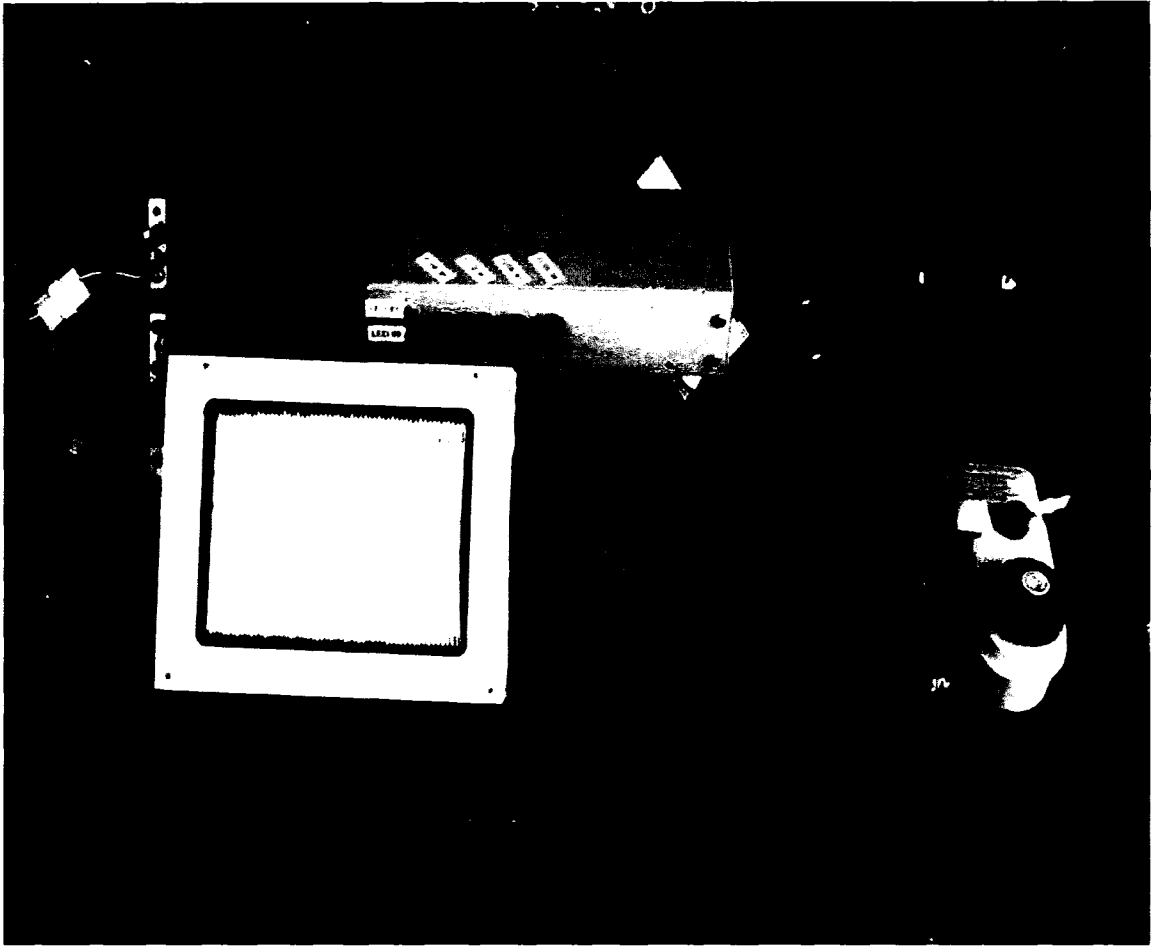


Figure 5-4 Relay box position under hood of Polaris vehicle

Fuel System

The fuel system conversion required removal of pre-existing tanks, fuel and carburetor. A throttle body was manufactured to replace the carburetor as well as to incorporate the throttle position and vacuum port for the MAP sensor. The fuel tank came pre-installed with a dispensing solenoid with built-in pressure relief device and thermocouple. To protect the occupants and or pedestrians, a low pressure relief system was installed to safely vent hydrogen in the event of an over pressurized occurrence due to pressure regulator failure, fire damage or mechanical damage or if the dump valve is

opened for any reason. Pictured in Figure 5-5 is the plumbing setup for the low pressure system.

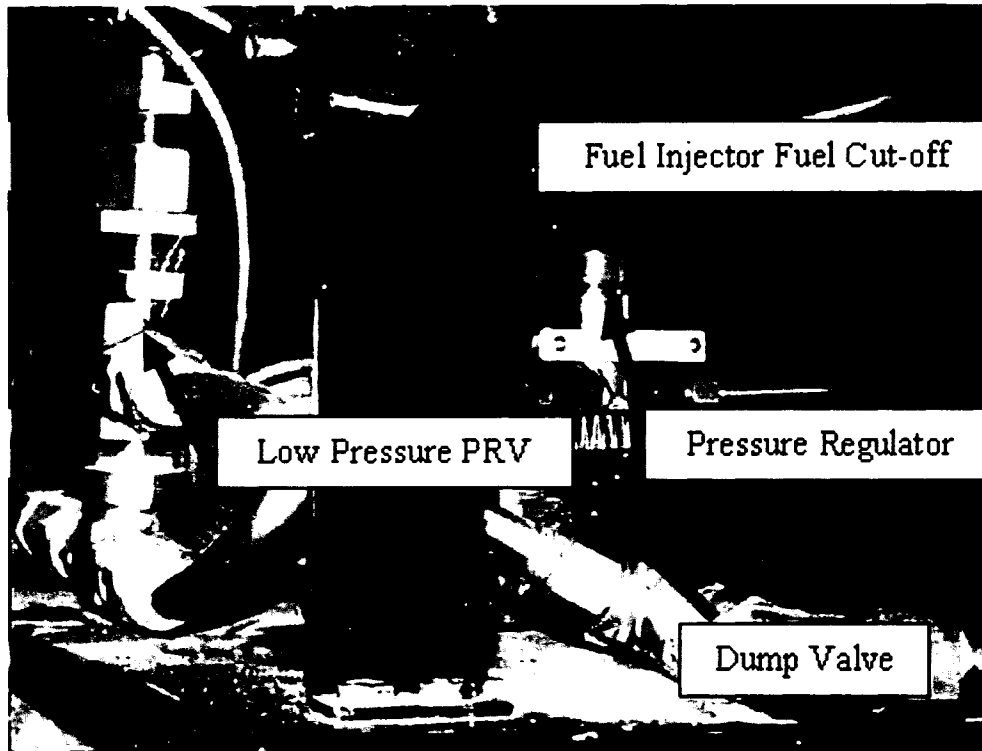


Figure 5-5 Polaris fuel cutoff valve, pressure regulator, dump valve and PVD

A standardized filling nozzle from OPW was installed on the passenger side for ease of filling. In the event that the users had need to fill from a non-standard dispenser such as a high pressure bottle, a secondary fill nozzle was also installed in line to the fuel tank. Pictured in Figure 5-6 is the mechanical pressure gauge, OPW fill nozzle and secondary fill adapter.

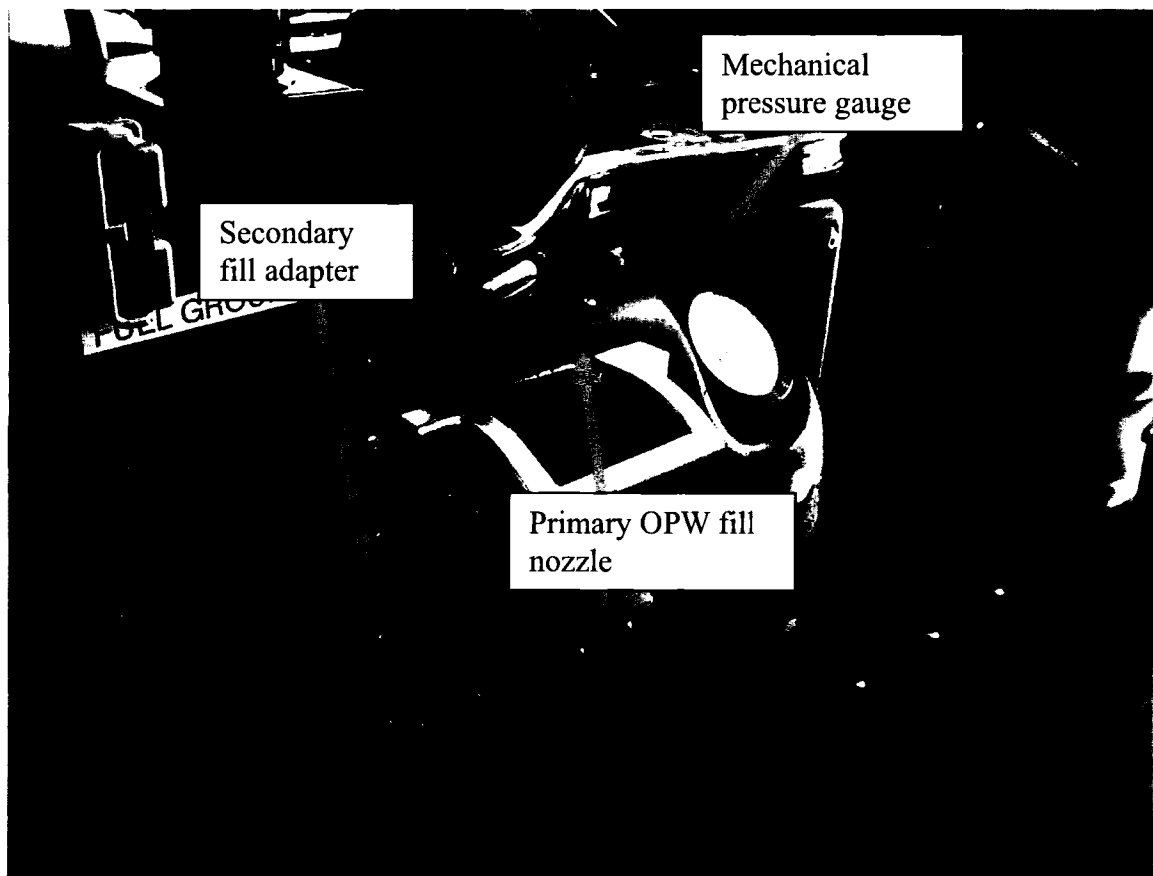


Figure 5-6 Fill connector and tank pressure gauge on Polaris vehicle

Ford Conversion

The Ford vehicle was originally outfitted to operate on CNG and was equipped with tanks, regulators, and plumbing. Because gaseous hydrogen is to be stored at 5500 psig, all plumbing, tanks, and regulator systems used for the CNG were removed. To date, all tanks (5 in total) have been mounted onto the bed of the pickup as well as all fuel lines running to both the engine and fuel cell have been installed. Pictured below is the unaltered vehicle into which the sparkplug injector fuel system will be installed.

The Ford vehicle, in addition to external sensors for fuel pressure, hydrogen gas sensors, relay control box with shutdown sequencer, required modifications for the injector wire harness. The injector harness modification consists of a voltage step-up

transformer from 12 VDC to 24 VDC and a injector control circuit from Kell's Automotive. The control circuit ensures the collapsing field from the large solenoid will not discharge into the ECM.



Figure 5-7 Ford vehicle to be converted

CHAPTER 6

TESTING AND ANALYSIS

Testing of the engines consisted of two parts: performance and emissions analysis. Performance was measured through the use of a dynamometer, mass flow meters, EGT sensors, and O₂ sensors. Testing of both types of injection system were conducted on the Polaris engine. For the case of the Ford engine, later studies will be performed to evaluate performance and emissions. Testing of the Polaris motor consisted of coupling the Dynamite dynamometer directly to the crankshaft whereas evaluation of the Ford will be done using a chassis dynamometer. Emissions were collected and evaluated using an ECOM Emissions Analyzer measuring CO, NO, and NO₂. Various other instruments used to evaluate and tune the engines are listed in Table 6-1.

Performance

Tuning of the engine involved coupling performance with emissions to ensure a power output is not maintained at the expense of emissions and vice versa. To ensure performance was not overly diminished by tuning for emissions requirements, various calculations such as BSFC, fuel burn efficiency, and brake mean effective pressure were used as a guideline. In general terms the performance criteria were defined as the maximum torque at a given engine speed and load which had the lowest possible emissions while maintaining a BSFC of 0.20 or better, a fuel burn efficiency of at least 20% and a BMEP of at least 100 psi for WOT and max engine speed. Performance was

evaluated by comparing the BSFC, power and torque curves. Evaluation of these categories was performed for gasoline, natural gas and hydrogen gas. The BSFC is generally used to evaluate the efficiency of the fuel burn whereas the torque and power curves generally represent engine characteristics such as cam profile, cylinder displacement, connecting rod lengths, etc. Table 6-1 represents the baseline testing of gasoline and CNG as compared to direct injection of hydrogen for near-stoichiometric conditions.

$$\text{BMEP} = \frac{150.8 \text{ Torque}}{\text{Displacement}} \quad (6-1)$$

The second law of thermodynamics (Equation 6-2) is an idealized case wherein friction losses are neglected, a fundamental limit can be calculated for the maximum efficiency. Using the adiabatic flame temperature as the ideal case for if not heat were lost via friction, pressure leaks, etc, the calculated engine efficiency is calculated to be 89%. By using the EGT, which would be closer the real world situation, the maximum engine efficiency is calculated to be 73%

$$\eta_{\text{Carnot}} = 1 - \frac{T_{\text{cold}}}{T_{\text{hot}}} \quad (6-2)$$

Using the LHV of each fuel (Table 6-2), the efficiency of the fuel burn is then calculated by Equation 6-3. The fuel burn efficiency is a comparison of the energy contained within a particular fuel and the amount of energy outputted. Table 6-1 summarizes this data for hydrogen using direct injection, CNG and Gasoline using port injection. Due to the wide flammability limit ranging from 4% to 70% for hydrogen,

emissions took precedence over performance at idle due to the ability to operate the engine extremely lean (AFR of 344 for a 4% concentration by volume). For this reason, it is possible to achieve a BSFC in the low 0.10 to 0.15 range at idle. This is reflected in Table 6-3 by a fuel burn efficiency of over 40%. As the engine is loaded and the RPM increases above the stall limit of the centrifugal clutch of the vehicle (1500 to 1600 RPM) power output is more critical to get the vehicle moving. For this reason, emissions requirements were backed off and performance standards mentioned previously were reinstated.

$$\eta_{\text{Fuel}} = \frac{1}{\text{LHV} \cdot \text{BSFC}} \quad (6-3)$$

Table 6-1 BSFC of various fuels at WOT

RPM	Hydrogen	CNG	Gasoline
1200	0.12	0.30	0.52
2000	0.18	0.31	0.51
2500	0.20	0.30	0.51
3000	0.19	0.32	0.52
3500	0.23	0.31	0.48
4000	0.22	0.30	0.45

Table 6-2 LHV of fuels

Fuel	Value (Hp*hr/ lb)
CNG	8.621
Gasoline	7.236
Hydrogen	20.208

Table 6-3 Engine efficiency of various fuels at WOT using BSFC and LHV

RPM	Hydrogen	CNG	Gasoline
Idle	41.24%	38.66%	26.25%
2000	27.65%	37.42%	26.77%
2500	24.53%	38.66%	26.77%
3000	25.48%	36.25%	27.30%
3500	21.52%	37.42%	28.44%
4000	22.49%	38.66%	30.33%

The volumetric efficiency of the motor can also be calculated using the BSFC and general parameters of the engine. Equation 6-4 was used to calculate the volumetric efficiency as a function of the AFR, power output, and mass flow of air through the engine.

$$VE = \frac{Hp \cdot BSFC \cdot t \cdot AFR}{\rho_{Air} \cdot Vol_{max}} \quad (6-4)$$

The following graphs represent the fuel burn and volumetric efficiency of each fuel. As a general rule, the maximum torque is achieved at the maximum volumetric efficiency. This phenomenon can be seen in all tested fuels, but it is more pronounced

with the hydrogen. The fuel efficiency is dependent upon the AFR whereas the volumetric efficiency is dependent upon the geometry of intake system. This too can be seen in the hydrogen test where idle to 2000 RPM operated at an equivalence ratio of approximately 0.75.

The volumetric and fuel burn efficiencies have also been computed for CNG and gasoline as shown in Figures 6-2 and 6-3. An indication of a poorly designed intake system, without positive pressure feed of the air supply, is a relatively low volumetric efficiency. Volumetric efficiencies in this particular motor do not exceed 80%. Fuel burn efficiency is a good indication of the amount of energy from the fuel that is used to produce power, the remaining energy that is unused is assumed to be lost as heat or blow-by of the compression rings.

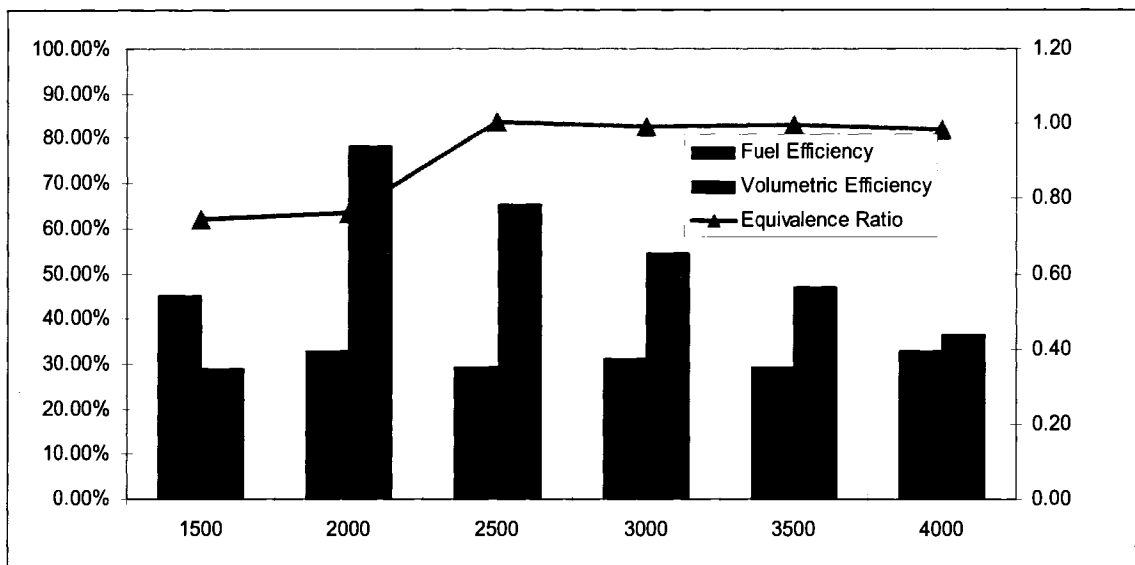


Figure 6-1 Fuel and volumetric efficiencies for hydrogen at WOT

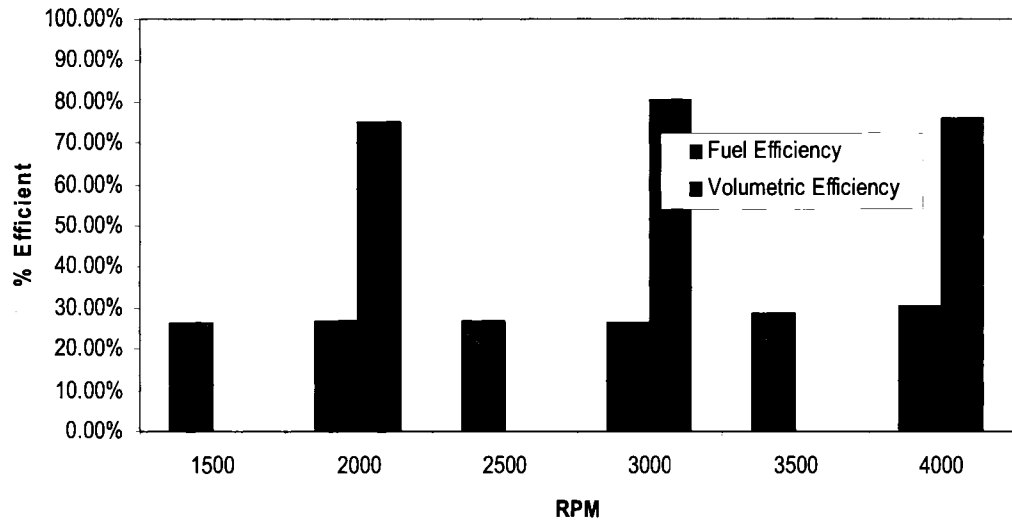


Figure 6-2 Volumetric and fuel efficiencies for gasoline at WOT, $\Phi = 1$

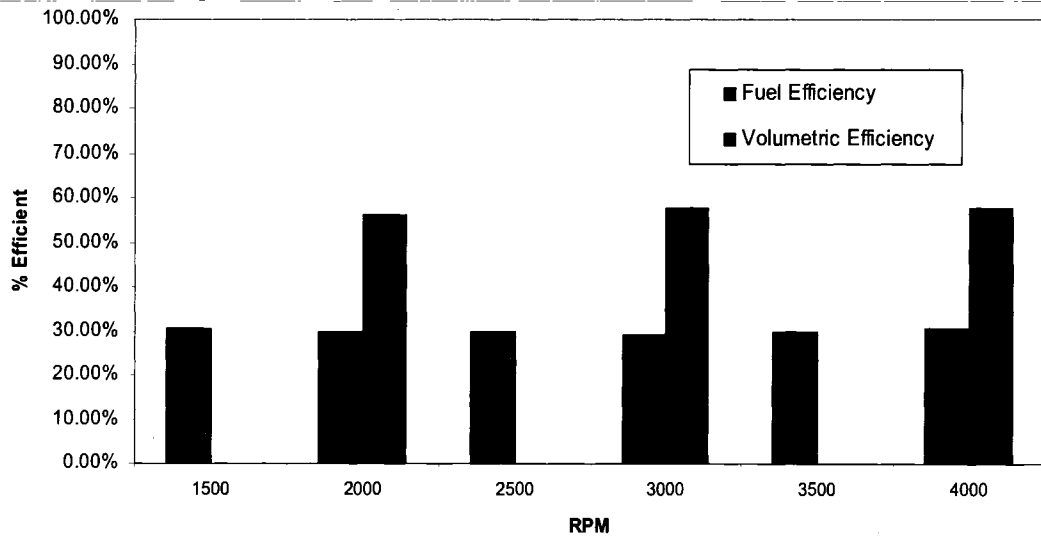


Figure 6-3 Volumetric and fuel efficiencies for CNG at WOT, $\Phi = 1$

The power levels of all fuels and configurations, i.e. port injection for all fuels and direct injection of hydrogen have been computed using SAE J1349 JUN90 correction factors. For comparison of all configurations, Figure 6-4 depicts power levels at WOT for varying engine speeds.

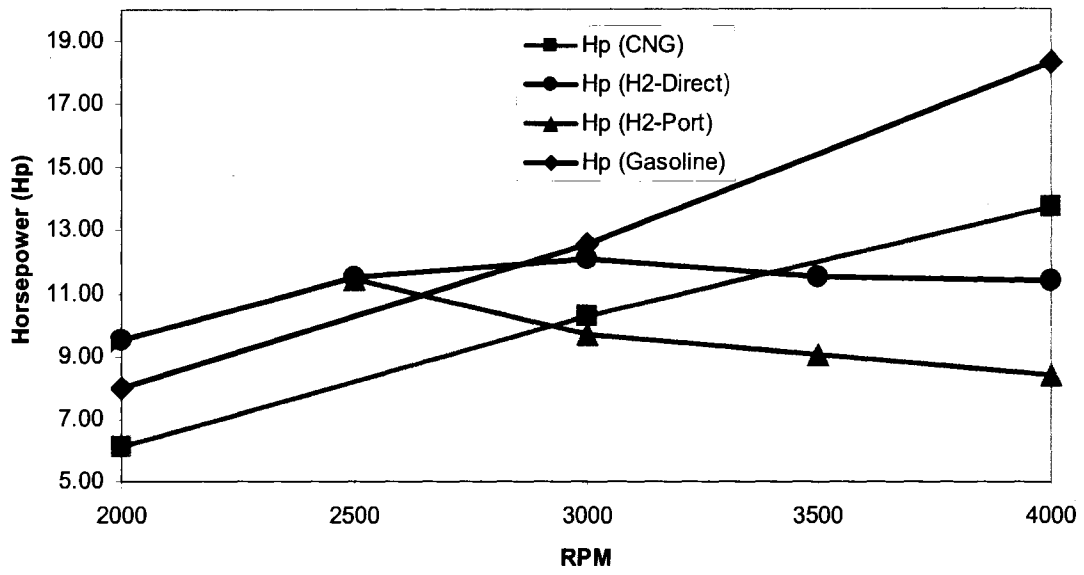


Figure 6-4 Power output of hydrogen, CNG and gasoline

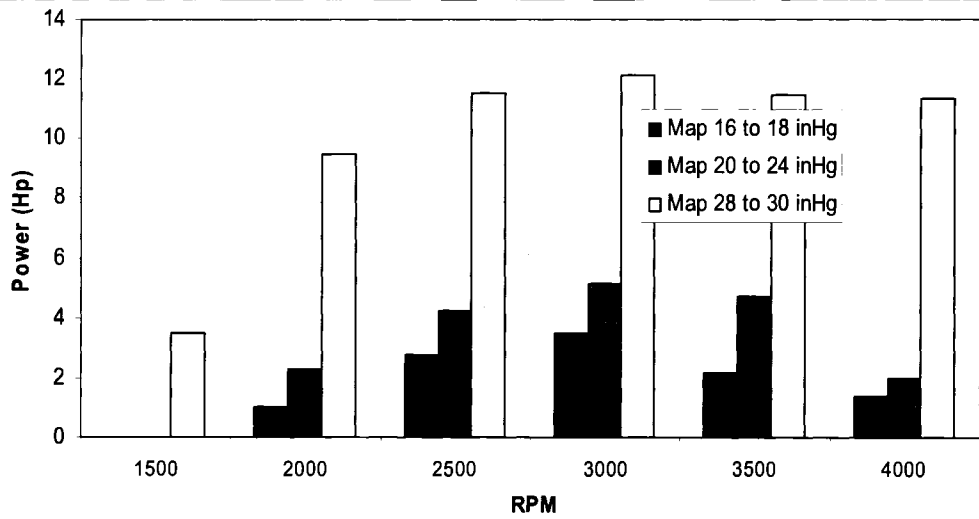


Figure 6-5 Power output for direct injection of hydrogen

Emissions

As the BSFC was chosen based on fuel efficiency and AFR, two remaining criteria for the configuration of an optimized engine are; 1) maximum power levels at 2) lowest possible emissions. Baseline testing for the original configuration as well as initial computer setup was performed for gasoline. To simulate a baseline for a gaseous fuel, natural gas was also tested. To justify the conclusion that maximum power occurs at stoichiometric conditions, various tests were performed to show power levels, and the effect of emissions at varying equivalence ratios.

Baseline Emissions Testing

Emissions for gasoline were taken in a series of two runs; the first at 3000 RPM and the second at 4000, both at WOT. For comparison these set of runs were taken at an equivalence ratio near 1.

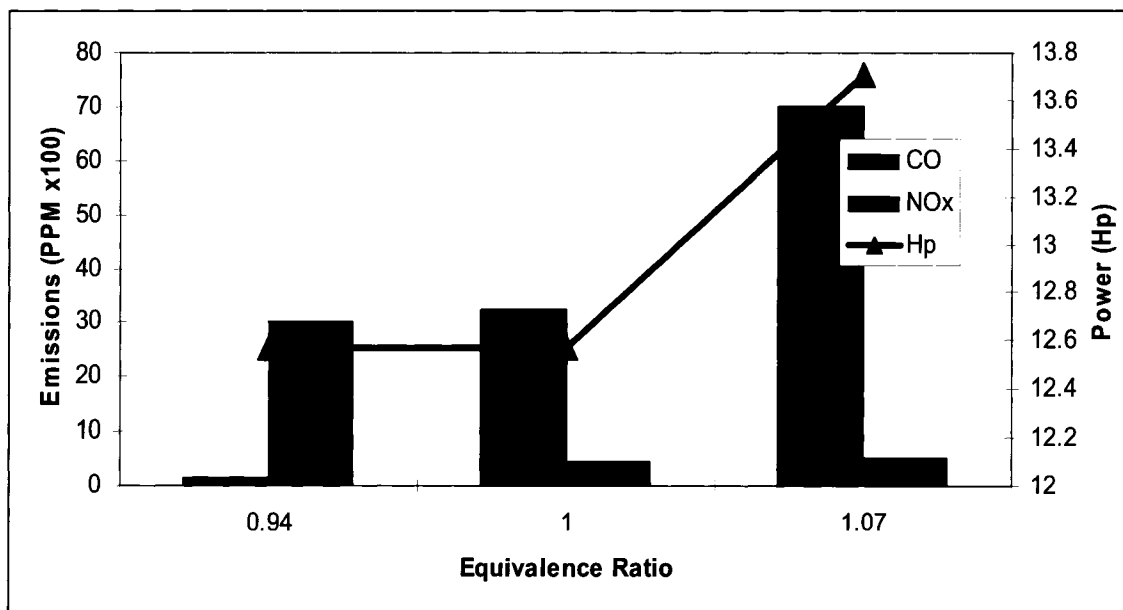


Figure 6-6 Emissions for gasoline at WOT, RPM = 3000

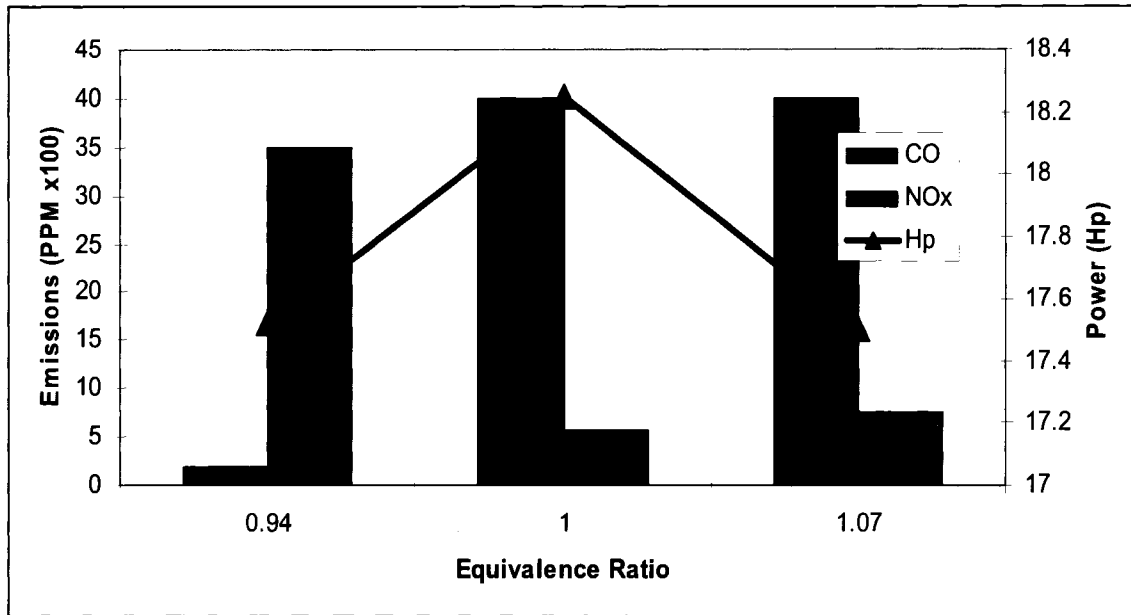


Figure 6-7 Emissions for gasoline at WOT, RPM = 4000

Emissions for CNG were taken in a series of two runs; the first at 3000 RPM and the second at 4000 both at WOT. For these series of runs the equivalence ratio was set to 0.96, 1.0 and 1.05 in order to verify proper tuning.

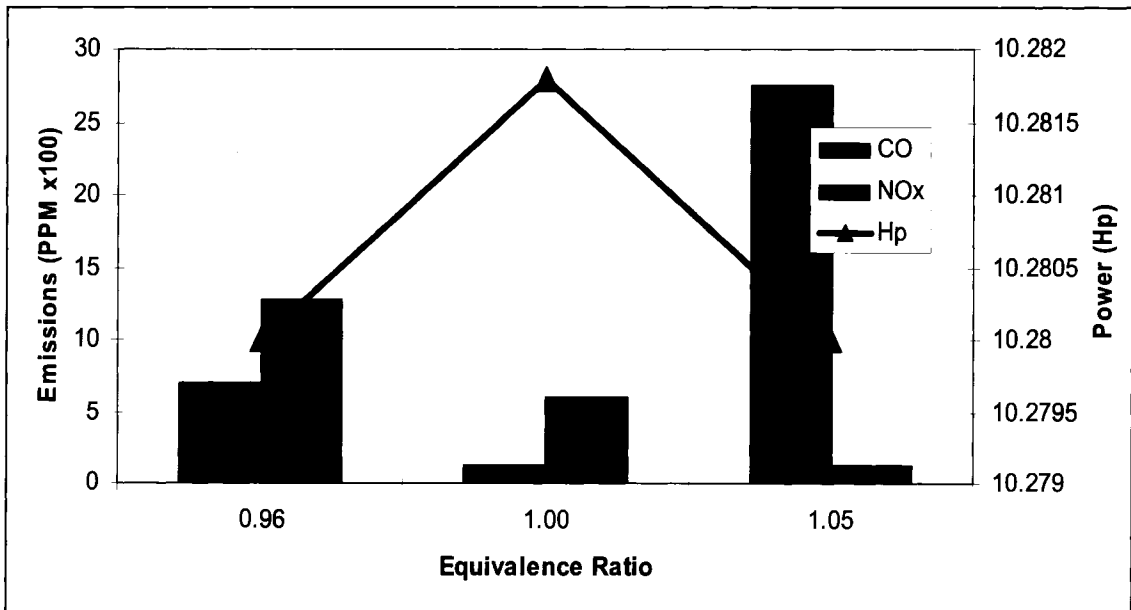


Figure 6-8 Emissions for CNG at WOT, RPM = 3000

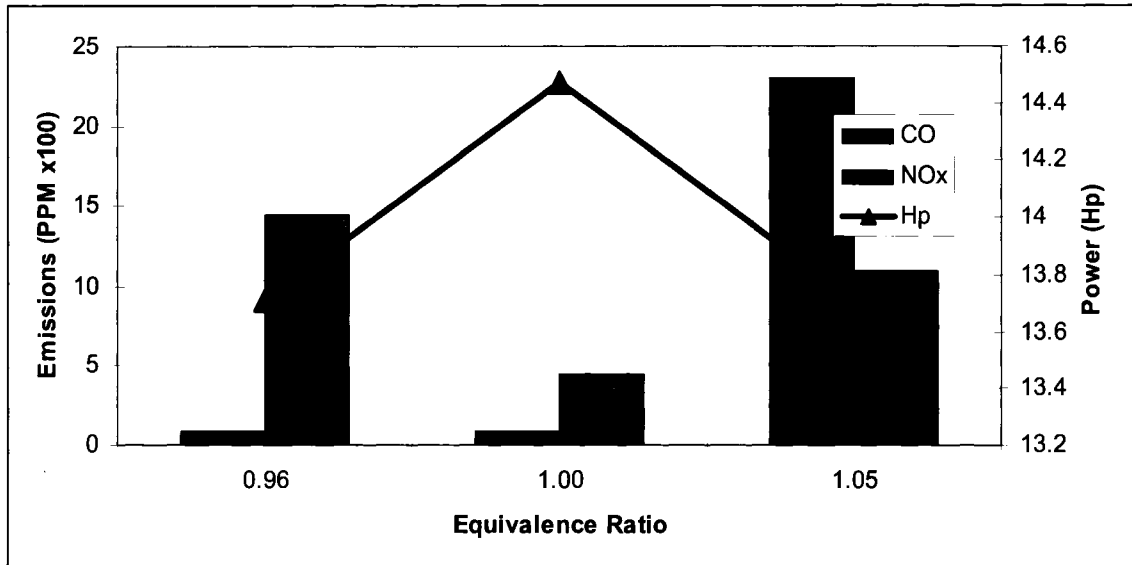


Figure 6-9 Emissions for CNG at WOT, RPM = 4000

Emissions for Direct Injection of Hydrogen

The following Figures represent data taken from various runs for direct injection of hydrogen. Data were taken at varying manifold pressures (indicating engine loads) at nearly constant BSFC values. The exception to the constant BSFC is at idle and up to 2000 RPM where no power is needed due to the transmission setup. It is recognized that emissions for these points take precedence over maximum power output. The procedure for taking emissions and power levels was to:

- Step 1) Achieve maximum power at a given AFR. Injection timing is set to 20° after the intake valve closes to give the maximum possible mixing time
- Step 2) Adjust spark to achieve spark timing range (typically 10° to 15°) wherein the BSFC criteria is obtained
- Step 3) Adjust spark timing within range set in Step 2 wherein emissions levels are minimized.

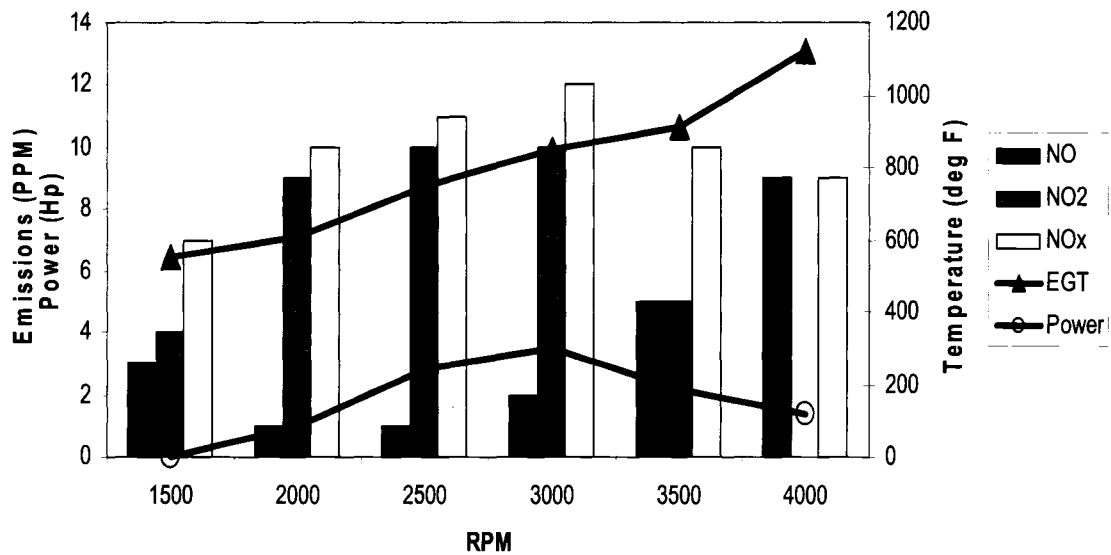


Figure 6-10 Emissions for direct injection of hydrogen at MAP = 16 to 18 inHg

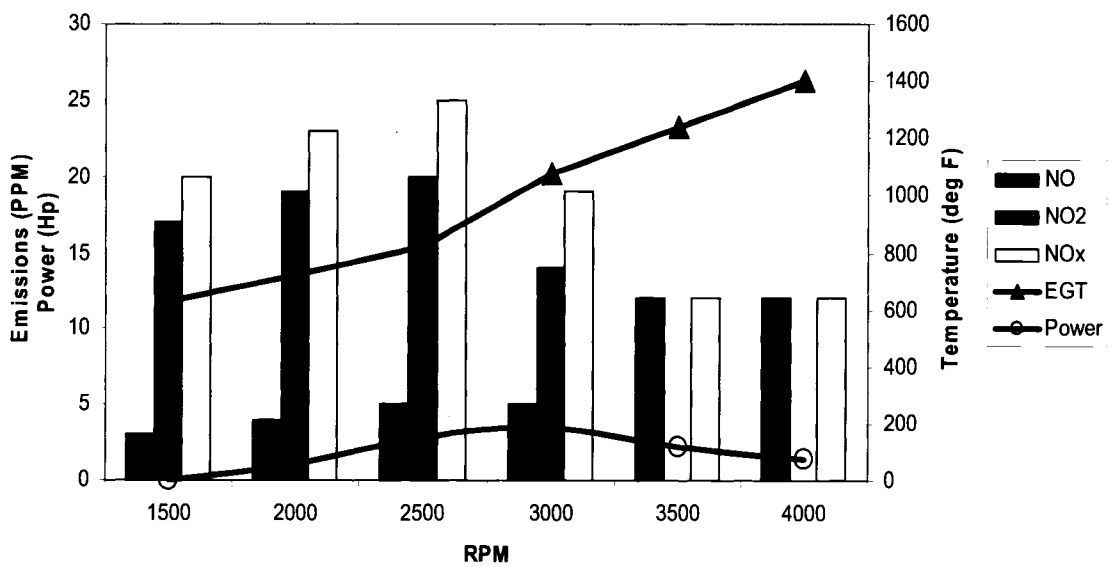


Figure 6-11 Emissions for direct injection of hydrogen at MAP = 20 to 24 inHg

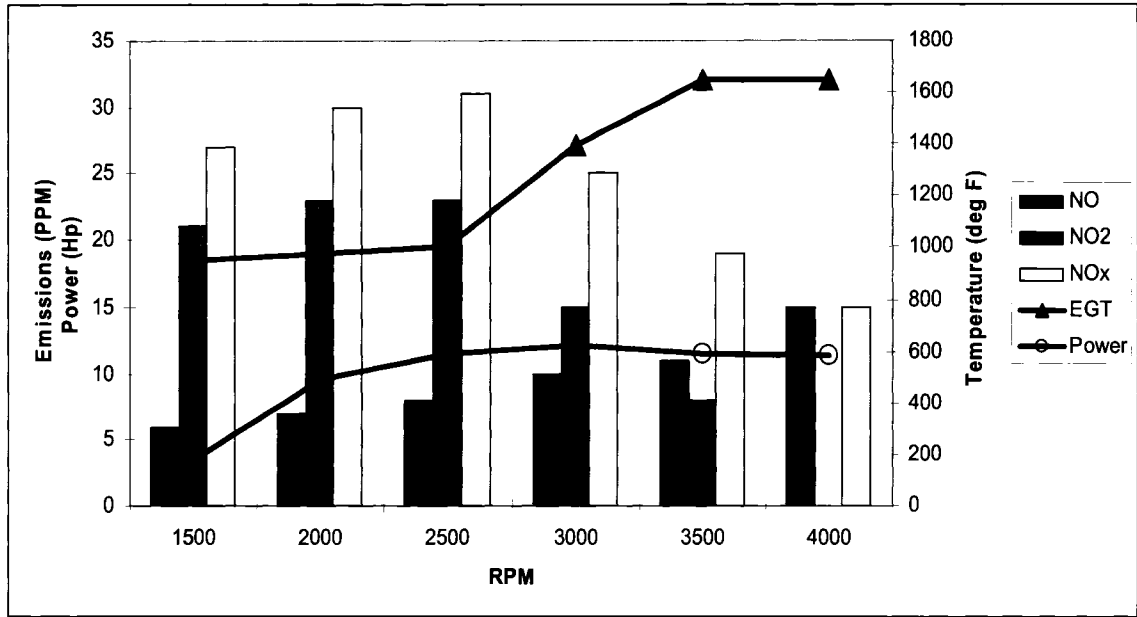


Figure 6-12 Emissions for direct injection of hydrogen at WOT

CHAPTER 7

DISCUSSION AND CONCLUSIONS

Literature reviews into hydrogen embrittlement, previous types of engine conversions, and different design techniques for solenoids give great insight into a development problem that could not be otherwise completed without the aid of many experiments. By studying hydrogen embrittlement, the mechanism of failure and subsequently the material(s) better suited for use in such application becomes clear.

While major components within the engine are made of aluminum, and aluminum is extremely susceptible to hydrogen embrittlement, it goes without saying that most if not all these parts cannot be substituted, however, planning which material will be used for components added such as the injector and check valve is one major step into avoiding catastrophic failures. Some failures cannot be avoided and so safety precautions can be implemented to help alleviate this problem. In the event of a failure within the combustion chamber, such as ring or piston failure, a blow-off valve as depicted in Figure 4-5 will purge excess pressure caused from the ignition of hydrogen within the crankcase. Likewise, to prevent damage to the MAP sensor a secondary blow-off valve has been installed on the intake system.

A traditional method for converting an engine to operate on hydrogen typically utilizes port injection. While port injection tends to have higher thermal efficiencies a loss of flame control results in pre-ignition and backfires thus resulting in a loss of power.

By use of direct injection higher volumetric efficiencies, better flame control and power densities comparable to that of gasoline can be achieved. The design of two injection units capable of delivering hydrogen into an ICE by means of direct injection have been designed, manufactured, tested, and used in the conversion of two vehicles. While it is shown that removal, modification, and reassembly of a cylinder head for the purpose of insertion of an injector into the cylinder head is a viable method, use of a preexisting passage such as the sparkplug hole is less labor intensive and has the advantage of testing numerous designs without the need for complete engine disassembly.

Several papers containing the development of a high speed solenoid were studied in order to better grasp the main concepts which ensure a reliable and fast responding solenoid capable of delivering adequate fuel control to the engine. Better understanding of reluctance and the important role it plays on the flux density was used in the development of the solenoid valves used in these conversions. Design of an internal solenoid is a possible alternative to mounting an external solenoid, and has been experimentally shown in lab settings to produce desired results. However, due to the limited space on the engine and time needed for various derivations of the design, namely time needed to condense the size of the solenoid valve, use of an internal solenoid was substituted for a simpler setup. Issues that needed to be addressed for a setup involving an external solenoid were response times needed for turn-on and additional time constants to ensure complete flow cut off. The external solenoid required an increased effective tube length to connect the valve portion of the solenoid to the injection point (approximately 10 inches in total). The increase in length requires additional time needed to deliver fuel. This increased time resulted in additional programming to ensure the exact amount of

fuel is delivered in the allotted time slot. For example, an engine rotating at 1500 RPM has a typical time between the closing of the intake valve and TDC of 11 ms whereas the engine rotating at a speed of 4500 RPM has a time of 3.7 ms.

Typical methods for reducing emissions can be accomplished by a number of methods. The most successful method is to operate the engine at a lean state (typically around 70:1), however this method results in a loss of power output due to less fuel involved in the combustion process. Another method commonly used even in gasoline engines is to operate the engine with an EGR system, which in effect lowers the combustion temperature thus reducing production of NO_x. This method has a tendency to lower the volumetric efficiency by reintroducing exhaust gasses for re-burning thus also reducing the maximum possible power output. The method of choice, given the small displacement of the Polaris engine is to operate the engine at near stoichiometric and to utilize a catalytic converter down stream of the exhaust. The advantage with this setup is max power is achieved and emissions are improved via an external device that will not effect the power output. By choosing specific regions such as low load for any RPM range as well as at idle to operate lean, fuel economy is improved while not at the expense of power output. As evident in Figures 6-6 through 6-9, emissions were generally lowest at a lean state. Maximum power was achieved at stoichiometric for all tests with the exception of gasoline at 3000 RPM. It is not entirely clear as to why power continues to increase for gasoline at 3000 RPM. It could be hypothesized that with an equivalence ratio greater than one and more fuel consumed led to a cooling of the combustion chamber thus resulting in higher power.

Programming schemes aimed at emission control for the Ford motor can vary from utilization of an EGR system, catalytic converter as these systems were factory integrated into the vehicle. Operation similar to the Polaris programming scheme is also possible. The most effective solution would be to operate the engine at an AFR of 70:1. This is only possible due to the significantly higher displacement and the ability of aftermarket parts such as superchargers. The purpose of a supercharger is to utilize the mechanical advantage of the engine to boost the volume and pressure of the air through the intake system. This creates a condition where there is more air within the combustion chamber which allows for two scenarios to play out. The first is an increase in power output by increasing the amount of fuel whereby the AFR remains the same. The second option is to keep the amount of fuel the same allowing a more efficient fuel burn thus leading to a very slight increase in power with operation at a lean state. The most economical, fuel saving, lowered emissions method would be to operate at a much leaner fuel mixture. This would achieve similar power levels when compared to the same engine operating without a supercharger with a fraction of the fuel needed.

APPENDIX I

TABLES OF ENGINE PARAMETERS AND C_v TEST RESULTS

Table AI-1 Specifications for 425cc Polaris engine

Engine specifications			
Platform		Fuji 4-stroke, single cylinder	
Engine Displacement		425cc	
Bore & Stroke (mm)		87.9 x 70	
Compression Ratio		9.2:1	
Intake Valve	Open	310 ATDC	
	Close	620 ATDC	
Exhaust Valve	Open	109 ATDC	
	Close	409 ATDC	

Table AI-2 Polaris check valve flow data for air

Inlet Pressure (PSIG)	Pressure Drop (PSIG)	Mass Flow Rate (lb/hr)	C_v
30	23.6	2.72	0.368
40	24.7	4.18	0.415
50	26.3	5.28	0.407
60	27.8	6.12	0.382
70	28.9	7.05	0.370
80	30.5	7.78	0.348
90	33.1	8.71	0.332
100	35.2	9.53	0.317

Table AI-3 Check valve seat test data

	Run 1	Run 2	Run 3	Run 4	Run 5
Seat material	Alloy 901	Alloy 901	673	673	C27 Bronze
Guide material	630	630	673	673	C27 Bronze
Plunger material	630	303 SS	303 SS	630	303 SS
Start depth (x 1/1000)	92.5	103.5	33.5	19	38.5
End depth (x 1/1000)	92.5	103.5	33.5	18	38
Testing time (hr)	2	2.5	1	1.5	6
Maximum Temp (°F)	160	145	141	175	142
Minimum Temp (°F)	135	110	104	110	99
Average Temp (°F)	145	140	125	115	120
Movement (0.001"/hr)	0	0	0	0.667	0.083
Maximum movement (in)	0.065	0.065	0.065	0.065	0.065
Time to failure (hr)	NA	NA	NA	97.5	780

APPENDIX II

MATHCAD SIMULATION OF EMISSIONS FOR 425CC ENGINE

Define Variables:

$$\begin{aligned} \text{AFR} &:= 50 & \text{Cp}_{\text{Air}} &:= 1.005 & \text{Cv}_{\text{Air}} &:= 0.72 \\ \text{Temp} &:= 90 & \text{Cp}_{\text{H}_2} &:= 14.307 & \text{Cv}_{\text{H}_2} &:= 10.18 \end{aligned}$$

Define Constants:

$$\begin{aligned} \text{mw}_{\text{H}_2} &:= 2.0159 && \text{(Molecular weight of Hydrogen)} \\ n_{\text{Air}} &:= 1 && \text{(Moles of Air)} \\ \text{CR}_{\text{eff}} &:= 6.33 && \text{(Effective Compression Ratio)} \\ \text{mw}_{\text{Air}} &:= 28.8623 && \text{(Molecular weight of Air)} \\ h_{\text{s_H}_2\text{O}} &:= -241820 && \text{(Enthalpy of formation for water)} \\ h_{\text{s_NO}} &:= 90300 && \text{(Enthalpy of formation for NO)} \end{aligned}$$

Define table of Enthalpy and Equilibrium using a 6th order curve fit ($R^2 = 0.999$ or better) (Tables from Moran Shapiro (A-23, A-25 and A-27))

$$\begin{aligned} h_{\text{NO}}(T) &:= 3.84283638 \cdot 10^{-11} \cdot T^4 - 6.04301031 \cdot 10^{-7} \cdot T^3 + 3.58832287 \cdot 10^{-3} \cdot T^2 + 2.82756591 \cdot 10^1 \cdot T - 8.92931176 \cdot 10^3 \\ h_{\text{H}_2}(T) &:= -1.04890056 \cdot 10^{-10} \cdot T^4 + 6.75725575 \cdot 10^{-7} \cdot T^3 + 3.24569056 \cdot 10^{-4} \cdot T^2 + 2.81780598 \cdot 10^1 \cdot T - 8.4492207 \cdot 10^3 \\ h_{\text{H}_2\text{O}}(T) &:= -2.5054243 \cdot 10^{-10} \cdot T^4 + 9.23093879 \cdot 10^{-7} \cdot T^3 + 4.37092424 \cdot 10^{-3} \cdot T^2 + 3.07130235 \cdot 10^1 \cdot T + 2.2149318 \cdot 10^2 \\ h_{\text{N}_2}(T) &:= -6.19102714 \cdot 10^{-11} \cdot T^4 - 3.99919871 \cdot 10^{-8} \cdot T^3 + 2.81766583 \cdot 10^{-3} \cdot T^2 + 2.72992673 \cdot 10^1 \cdot T + 1.82727765 \cdot 10^2 \\ h_{\text{O}_2}(T) &:= 1.45873502 \cdot 10^{-10} \cdot T^4 - 1.34835576 \cdot 10^{-6} \cdot T^3 + 5.63128702 \cdot 10^{-3} \cdot T^2 + 2.68544143 \cdot 10^1 \cdot T + 1.08996076 \cdot 10^2 \\ K_{\text{NO}}(T) &:= 10^{\left(\begin{aligned} &-4.49170418 \cdot 10^{-19} \cdot T^6 + 5.85738021 \cdot 10^{-15} \cdot T^5 - 3.07046519 \cdot 10^{-11} \cdot T^4 + 8.27081951 \cdot 10^{-8} \cdot T^3 - 1.21341085 \cdot 10^{-4} \cdot T^2 \dots \\ &+ 9.45470178 \cdot 10^{-2} \cdot T - 3.44662247 \cdot 10^1 \end{aligned} \right)} \\ K_{\text{H}_2\text{O}}(T) &:= 10^{\left(\begin{aligned} &-1.19598460 \cdot 10^{-18} \cdot T^6 + 1.55984810 \cdot 10^{-14} \cdot T^5 - 8.17899018 \cdot 10^{-11} \cdot T^4 + 2.20428817 \cdot 10^{-7} \cdot T^3 - 3.23741308 \cdot 10^{-4} \cdot T^2 \dots \\ &+ 2.52931657 \cdot 10^{-1} \cdot T - 9.17250833 \cdot 10^1 \end{aligned} \right)} \end{aligned}$$

Define Equations:

Balanced Chemical Equation

$$n_{\text{H}_2} \cdot \text{H}_2 + n_{\text{O}_2} \cdot \text{O}_2 + n_{\text{N}_2} \cdot \text{N}_2 = e \cdot \text{NO} + a \cdot \text{H}_2\text{O} + (n_{\text{H}_2} - a) \cdot \text{H}_2 + \left(n_{\text{N}_2} - \frac{1}{2} \cdot e \right) \cdot \text{N}_2 + \left(n_{\text{O}_2} - \frac{1}{2} \cdot e - \frac{1}{2} \cdot a \right) \cdot \text{O}_2$$

Dissociation Equations

$$\text{H}_2\text{O} = \text{H}_2 + \frac{1}{2} \cdot \text{O}_2$$

$$\frac{1}{2}O_2 + \frac{1}{2}N_2 = NO$$

Calculate moles of H_2 , O_2 and N_2 based on AFR and moles of Air

$$n_{H_2} := \frac{n_{Air} \cdot mw_{Air}}{mw_{H_2} \cdot AFR}$$

$$n_{O_2} := n_{Air} \cdot 21.14\%$$

$$n_{N_2} := n_{Air} \cdot 78.82\%$$

$$C_{p_{Mix}} := C_{p_{Air}} \frac{\frac{1}{mw_{Air}}}{\frac{1}{mw_{Air}} + \frac{1}{AFR \cdot mw_{H_2}}} + C_{p_{H_2}} \frac{\frac{1}{AFR \cdot mw_{H_2}}}{\frac{1}{mw_{Air}} + \frac{1}{AFR \cdot mw_{H_2}}} \quad (\text{Calculate } C_p \text{ of mixture})$$

$$C_{v_{Mix}} := C_{v_{Air}} \frac{\frac{1}{mw_{Air}}}{\frac{1}{mw_{Air}} + \frac{1}{AFR \cdot mw_{H_2}}} + C_{v_{H_2}} \frac{\frac{1}{AFR \cdot mw_{H_2}}}{\frac{1}{mw_{Air}} + \frac{1}{AFR \cdot mw_{H_2}}} \quad (\text{Calculate } C_v \text{ of mixture})$$

$$k := \frac{C_{p_{Mix}}}{C_{v_{Mix}}} \quad (\text{Calculate } k \text{ of mixture based on } C_v \text{ and } C_p \text{ of mixture})$$

Calculate final temperature and pressure based on polytropic process

$$P := CR_{eff}^k$$

$$T_f := \left[(Temp - 32) \frac{5}{9} + 273.15 \right] \cdot CR_{eff}^{k-1}$$

Energy equations

$$h_R := n_{H_2} \cdot h_{H_2}(T_f) + n_{O_2} \cdot h_{O_2}(T_f) + n_{N_2} \cdot h_{N_2}(T_f)$$

$$h_P = e \left(h_{s_NO} + h_{NO}(T) \right) + a \left(h_{s_H_2O} + h_{H_2O}(T) \right) + (2 - a) \cdot h_{H_2}(T) + \left(n_{N_2} - \frac{1}{2} e \right) \cdot h_{N_2}(T) \dots \\ + \left(n_{O_2} - \frac{1}{2} e - \frac{1}{2} a \right) \cdot h_{O_2}(T)$$

Setup solver for 3 equations and 3 unknowns:

Balanced chemical equation is redefined with coefficients as follows:

$$n_{H_2} \cdot H_2 + n_{O_2} \cdot O_2 + n_{N_2} \cdot N_2 = e \cdot NO + a \cdot H_2O + c(a) \cdot H_2 + d(e) \cdot N_2 + b(e, a) \cdot O_2$$

$$b(e, a) := n_{O_2} - \frac{1}{2} e - \frac{1}{2} a \quad c(a) := n_{H_2} - e$$

$$d(e) := n_{N_2} - \frac{1}{2} e \quad N(a) := n_{N_2} + n_{O_2} + \frac{1}{2} e$$

Guess

$$e := 0.001$$

$$a := 0.1$$

$$T := 2000$$

Given

$$\frac{c(a) \cdot b(e, a)^{\frac{1}{2}}}{a} \left(\frac{P}{N(a)} \right)^{\frac{1}{2}} = K_{\text{H}_2\text{O}}(T) \quad \text{(Equilibrium mixture equation for the dissociation of water)}$$

$$\frac{e}{b(e, a)^{\frac{1}{2}} \cdot d(e)^{\frac{1}{2}}} = K_{\text{NO}}(T) \quad \text{(Equilibrium mixture equation for the dissociation of NO)}$$

$$e \left(h_{s_NO} + h_{\text{NO}}(T) \right) + a \left(h_{s_H_2O} + h_{\text{H}_2O}(T) \right) + c(a) \cdot h_{\text{H}_2}(T) + d(e) \cdot h_{\text{N}_2}(T) + b(e, a) \cdot h_{\text{O}_2}(T) = h_R$$

Solution := Find(a, e, T)

APPENDIX III

TEST DATA FOR EXTERNAL COIL OPERATION AT 12, 18, AND 24 VDC

Table AIII-1 External coil at 12 VDC

Temp °F	Resistance	Current	t (min)	Voltage	P
105.0	10.53	1.14	0	12.05	13.73
146.0	11.62	1.03	5	12.05	12.44
159.6	12.04	1.00	10	12.05	12.01
166.5	12.26	0.98	15	12.05	11.80
172.2	12.44	0.96	20	12.04	11.61
177.5	12.62	0.95	25	12.04	11.44
179.1	12.68	0.95	30	12.04	11.39
181.3	12.76	0.94	35	12.03	11.32
182.5	12.80	0.94	40	12.03	11.28

Table AIII-2 External coil at 18 VDC

Temp °F	Resistance	Current	t (min)	Voltage	Power
132.0	11.23	1.59	0	17.9	28.54
200.0	13.45	1.33	5	17.9	23.82
206.4	13.71	1.31	7	17.9	23.37
209.8	13.85	1.29	8	17.9	23.14
215.1	14.07	1.27	10	17.9	22.77
223.5	14.44	1.24	13	17.9	22.19
226.2	14.56	1.23	16	17.9	21.99
230.0	14.74	1.20	19	17.7	21.25
236.0	15.03	1.18	26	17.7	20.84
234.0	14.93	1.08	30	16.2	17.57

Table AIII-3 External coil at 24 VDC

Temp °F	Resistance	Current	t (min)	Voltage	Power
107.0	10.58	2.32	0	24.6	57.18
150.0	11.74	2.10	1	24.6	51.54
203.0	13.57	1.81	3	24.6	44.59
236.0	15.03	1.64	5	24.6	40.26
261.8	16.41	1.50	8	24.6	36.88
277.1	17.35	1.42	10	24.6	34.87
282.0	17.68	1.39	14	24.6	34.23
285.4	17.91	1.37	16	24.6	33.79
287.3	18.05	1.36	19	24.6	33.54
289.2	18.18	1.35	21	24.6	33.29
287.1	18.03	1.36	23	24.6	33.56
288.0	18.09	1.36	25	24.6	33.44
288.4	18.12	1.36	27	24.6	33.39

APPENDIX IV

TEST EQUIPMENT

Table AIV-1 Testing instruments by manufacturer

Instrument	Manufacturer	Use
Air flow meter	Sierra Instruments	Mass flow rate of air entering intake manifold
Coriolis meter	Micro Motion Emerson	Mass flow rate of hydrogen fuel consumed
Air Fuel Meter	ECM	Calculated AFR based on wide range O ₂
Emissions Analyzer	ECOM	Measured CO, NO, and NO ₂ of exhaust
Polaris Dynamometer	Dynamite	Measured torque, calculated SAE corrected horsepower

REFERENCES

- [1] S. Serebrinsky, E.A. Carter, and M. Ortiz, "A quantum-mechanically informed continuum model of hydrogen embrittlement.", Journal of the Mechanics and Physics of Solids, volume 52 (2004), pages 2403-2430
- [2] Nelson H. G., "Hydrogen embrittlement." Treatise Mater Science Technology. No. 25 (1983) Pgs 275-359
- [3] Z. Hu, et al., "Hydrogen embrittlement of a single crystal of iron on a nanometer scale at a crack tip by molecular dynamics.", Modeling Simulation. Mater. Science Engineering, Volume 7 (1999), page 541-551
- [4] R. Smith, "Computer simulation of intergranular stress corrosion cracking via hydrogen embrittlement.", Modeling Simulation. Mater. Science Engineering, Volume 8 (2000), pages 629-648
- [5] Y. Kimura and K. Tsuzaki, Improvement of Hydrogen Embrittlement in a Tempered Martensitic Steel Through Grain Refinement Using Undissolved Cementite, University of Cambridge, 2005
- [6] M. Mayday, G. Filacchioni, and L. Pilloni, "A comparative study about the hydrogen Embrittlement susceptibility of Eurofer'97 and convectional 9%Cr ferritic/martensitic steels.", Fusion Engineering and Design, Volumes 75-79, November 2005, Pages 957-961 Proceedings of the 23rd Symposium of Fusion Technology - SOFT 23
- [7] R. K. Dayal, N. Parvathavarthini, "Hydrogen embrittlement in power plant steels.", Sadhana Volume. 28, Parts 3&4, June/ August 2003, Pgs 431-451
- [8] Albert S. K., et al., "Studies on susceptibility of 2-25Cr-1Mo Steels." Indian Welding Journal (1997) Pgs 7-13
- [9] Yurioko N, Sazuki H, "Hydrogen assisted cracking in C-Mn and low alloy steel weldments." International Mater: Rev. 35 (1990) Pgs. 217-249
- [10] P. V. Petroyiannis, et al., "Evidence on the corrosion-induced hydrogen embrittlement of the 2024 aluminum alloy.", Fatigue Fracture Engineering Material Strictures volume 28 (2005), pages 565-574
- [11] G. Lu and E. Kaxiras, "Hydrogen Embrittlement of Aluminum: The crucial role of vacancies." The American Physical Society 2005, Cambridge, Massachusetts

- [12] I. Huang and S. K. Yen, "Retardation effects of electrolytic ZrO₂ coating on hydrogen embrittlement of AISI 430 Stainless Steel", IEEE 1999 Pgs 425-428
- [13] Tang X, Kabat DM, Natkin RJ, Stockhausen WF. "Ford P2000 hydrogen engine dynamometer development." SAE Paper 2002; 2002-01-0242
- [14] Li H, Karim GA. "Knock in spark ignition hydrogen engines." International Journal: Hydrogen Energy 2004 Pgs 859-865
- [15] Maher AR, Sadiq AB. "Effect of compression ratio, equivalence ratio and engine speed on the performance and emission characteristics of a spark ignition engine using hydrogen as a fuel." Renewable Energy 2004 Pgs 2245-2260
- [16] N. Saravanan, G. Nagarajan, S. Narayanasamy, "An experimental investigation on DI diesel engine with hydrogen fuel" International Journal on Hydrogen Energy (2007) Volume 32
- [17] Lewis B, von Elbe G. "Combustion, flames, and explosions of gases." Orlando, Fl: Academic Press; 1987.
- [18] J. Lee, et al. "The development of a dual injection hydrogen fueled engine with high power and high efficiency." ASME-ICED 2002 Technical Conference. Sheraton New Orleans Hotel, New Orleans, LA
- [19] A. Mohammadi, et al. "Performance and combustion characteristics of a direct injection SI hydrogen engine." International Journal of Hydrogen Energy 32 (2007) volume 32, Issue 1 pgs. 296-304
- [20] T. Kajima, and Y. Kawamura, "Development of a high-speed solenoid valve: Investigation of solenoid." IEEE Transaction on Industrial Electronics, volume. 42, NO. 1, February 1995
- [21] B. Sung and E. Lee, "Optimal design of high-speed solenoid actuator using a non-magnetic ring." Electrical Machines and Systems, 2005. ICEMS 2005. Proceedings of the Eighth International Conference. volume 3, Pg 2333-2338
- [22] C. White, R. Steeper, A. Lutz, "The hydrogen-fueled internal combustion engine: a technical review", Science Direct: International Journal of Hydrogen, Energy 31, (2006) Pgs.. 1292-1305
- [23] Caton, Jerald A., Kim, Y. Y., and Lee, Jong T., 2002, "The Development of a dual injection hydrogen fueled engine with high power and high efficiency" ASME-ICED Technical Conference, 2002
- [24] T. Kishi, et al., "Characteristics of hydrogen combustion in an experimental lean premixed combustor." 2nd Symposium on Smart Control of Turbine (2001)

- [25] C. Chryssakis, D. Assanis, "Effect of multiple injections on fuel-air mixing and soot formation in diesel combustion using direct flame visualization and CFD techniques", ASME Internal Combustion Engine Division 2005 Spring Technical Conference, Paper number ICE2005-1016
- [26] K. Sapru, et.al, "Ovonic metal hydride based hydrogen ICE scooter", Proceedings of the 2001 Hydrogen Program Review, 2001
- [27] T. Shudo, K. Tsuga, "Analysis of direct injection SI stratified combustion in hydrogen lean mixture: Combustion promotion and cooling loss by hydrogen." International Journal of Automotive Technology, Volume 2, No. 3, Pgs.. 85-91 (2001)
- [28] T. Shudo, "Improving thermal efficiency by reducing cooling losses in hydrogen combustion engines." International Journal of Hydrogen Energy (2007) Volume 32, Issue 16
- [29] P. Aghalayam, P. Bui and D. Vlachos, "The role of radical quenching in flame stability and wall heat flux: hydrogen-air mixtures."
- [30] L. Eriksson, I. Andersson, "An analytic model for cylinder pressure in a four stroke SI engine." Society of Automotive Engineers 2002, Paper No. 2002-01-0371
- [31] M. Sadeghipour, Y. Razi, "Effects of confining wall on laminar natural convection from a horizontal cylinder." American Institute of Aeronautics and Astronautics 2000, Paper No. AIAA-2000-3026
- [32] S. Karagiorgis, et al., "Dynamic modeling of combustion and gas exchange processes for controlled auto-ignition engines." Proceeding of the 2006 American Control Conference, Minneapolis, Minnesota, USA, June 14-16, 2006. Pg 1880-1885
- [33] E. Urip, S. Yang, and O. Arici, "Conjugate heat transfer for internal combustion engine application using KIVA code." International Multidimensional Engine Modeling User's Group, Detroit. April 10,2005
- [34] A. Alkidas, "Combustion advancements in gasoline engines." Science Direct: Energy Conversion and Management (2007)
- [35] P. Falcone, et al. "Torque generation model for Diesel Engine." Proceeding of the 42nd IEEE Conference on Decision and Control, Maui, Hawaii USA, December 2003. Pgs. 1771-1776

- [36] L. Passarini and P. Nakajima, "Development of a high-speed solenoid valve: an investigation of the importance of the armature mass on the dynamic response." Journal of the Brazil Society of Mechanical Science and Engineers 2003
- [37] Z. Shengchang, et al., "Study on extra-high speed digital valve." Fifth International Conference On Fluid Power Transmission And Control (Icfp2001)
- [38] G. Nagu, Amarnath, and T. Namboodhiri, "Effect of heat treatment on the hydrogen embrittlement susceptibility of API X-65 grade line-pipe steel." Bull. Mater. Sci., volume 26 (2003), pages 435-439
- [39] Savannah River Technology Center, May 2003, Evaluation of Hydrogen Embrittlement of SAFKEG 3940A Package in KAMS, WSRC-TR-2003-00196, DOE contract # DE-AC09-96SR18500

VITA

Graduate College
University of Nevada, Las Vegas

Ronald L. Fifield

Home Address:

2471 Bench Reef Pl.
Henderson, Nevada 89052

Degrees:

Bachelor of Science, Mechanical Engineering, 2005
University of Nevada, Las Vegas

Publications:

R. Fifield, J. Gardner, R.F. Boehm, T. Kell, "Use of Direct Cylinder Injection in Hydrogen Engine Conversions", NHA Annual Hydrogen Conference 2007

R. Fifield, J. Gardner, R.F. Boehm, "Conversion and Performance Analysis of a Small Utility Vehicle Operating on Hydrogen Fuel", ASME Conference Proceeding, ASME Journal of Energy Resources Technologies 2007

J. Gardner, R. Fifield, R.F. Boehm, R. Hurt, Y. Baghzouz, "Design, Evaluation and Application of a Fuel Cell Vehicle", NHA Annual Hydrogen Conference 2007

R. Boehm, Y. Baghzouz, R. Hurt, R. Mauldin, E. Bulla, R. Fifield, and J. Gardner, "Development of a Renewably-Based Hydrogen Generation/Utilization System," International Solar Energy Conference, Denver, Colorado, 2006.

Thesis Title: Development of In-cylinder Injection for a Hydrogen-fueled Internal Combustion Engine

Thesis Examination Committee:

Chairperson, Dr. Robert Boehm, Ph. D.
Committee Member, Dr. Mohamed Trabia, Ph. D.
Committee Member, Dr. Woosoon Yim, Ph. D.
Graduate Faculty Reprehensive, Dr. Yahia Baghzouz, Ph. D.